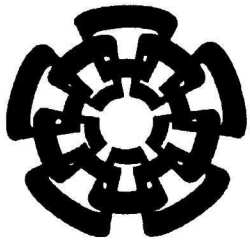

Centro de Investigación y de Estudios Avanzados

del I.P.N.

Unidad Guadalajara

Control Neuronal Descentralizado en Tiempo Continuo

Tesis que presenta:
Victor Hugo Benitez Baltazar

para obtener el grado de:
Doctor en Ciencias

en la especialidad de:
Ingeniería Eléctrica

Directores de Tesis:
Dr. Edgar Nelson Sanchez Camperos
Dr. Alexander Georgievich Loukianov

Guadalajara, Jalisco, Febrero de 2010.

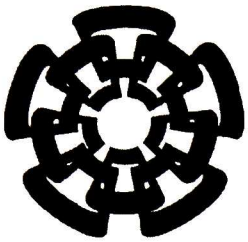

Centro de Investigación y de Estudios Avanzados

del Instituto Politécnico Nacional

Unidad Guadalajara

Decentralized Continuous Time Neural Control

A thesis presented by:
Victor Hugo Benitez Baltazar

to obtain the degree of:
Doctor in Science

in the subject of:
Electrical Engineering

Thesis Advisors:
Dr. Edgar Nelson Sánchez Camperos
Dr. Alexander Georgievich Loukianov

Guadalajara, Jalisco, February 2010

Control Neuronal Descentralizado en Tiempo Continuo

Tesis de Doctorado en Ciencias
Ingeniería Eléctrica

Por:
Victor Hugo Benitez Baltazar
Maestro en Ciencias en Ingeniería Eléctrica
Centro de Investigación y de Estudios Avanzados del IPN
Unidad Guadalajara 2000-2002

Becario de CONACYT, expediente no. 158003

Directores de Tesis:
Dr. Edgar Nelson Sánchez Camperos
Dr. Alexander Georgievich Loukianov

CINVESTAV del IPN Unidad Guadalajara, Febrero, 2010.

Decentralized Continuous Time Neural Control

Doctor of Science Thesis
In Electrical Engineering

By·
Victor Hugo Benitez Baltazar
Master of Science in Electrical Engineering
Centro de Investigación y de Estudios Avanzados del IPN
Unidad Guadalajara, 2000-2002

Scholarship granted by CONACYT, No. 158003

Thesis Advisors:
Dr. Edgar Nelson Sánchez Camperos
Dr. Alexander Georgievich Loukianov

CINVESTAV del IPN Unidad Guadalajara, February, 2010.

Resumen

La tesis está dirigida al desarrollo de un esquema de identificación y control descentralizado basado en redes neuronales recurrentes de alto orden (*RHONN* por sus siglas en inglés) y su aplicación a sistemas de gran escala. Muchos sistemas, tales como la red eléctrica de potencia, redes de computadoras y de telecomunicaciones, redes de sistemas dinámicos, sistemas de transporte, sistemas de manufactura, industria de procesos y muchos otros, son sistemas interconectados de gran escala.

Para controlar dichos sistemas, se han propuesto en la literatura esquemas de control centralizado, suponiendo que se tienen disponible toda la información de las dinámicas del sistema. A pesar de que hay ventajas teóricas obvias, la centralización de la ley de control es muy difícil para un sistema complejo de gran escala con interconexiones debido a razones técnicas y económicas. Más aún, los diseños de control centralizado son dependientes de la estructura del sistema y no pueden manejar cambios estructurales. Si se agregan o eliminan subsistemas, el controlador para el sistema global debe ser rediseñado.

El enfoque de control descentralizado surge a partir de la alta dimensión del sistema a ser controlado, la imposibilidad en el intercambio de información entre subsistemas, la falta de capacidad de cómputo requerido en el caso de un único controlador central y la incertidumbre en la medición de parámetros dentro de un sistema de gran escala.

En esta tesis se establece la viabilidad de aplicar redes neuronales recurrentes de alto orden (*RHONN*) como identificadores adaptables de los subsistemas de gran escala usando únicamente la información disponible localmente. Se consideran como perturbaciones los términos de interconexión y se investiga la implementación de un controlador discontinuo usando la teoría de control de estructura variable. Los algoritmos desarrollados se aplican a diversos sistemas electromecánicos, y los resultados se muestran en simulación y se verifica la aplicabilidad de los algoritmos propuestos para sistemas electromecánicos interconectados.

Abstract

This thesis deals with the development of decentralized identification and control algorithms based on recurrent high order neural networks and its applicability to large scale systems. Many physical systems, such as power grid, computer and communication networks, networked dynamical systems, transportation systems, manufacture systems, processes industry and many others, are complex large-scale interconnected systems.

To control such large scale systems, centralized control schemes are proposed in the literature assuming available global information for the overall system. While there are obvious theoretical advantages, control centralization is very difficult for a complex large scale system with interconnections due to technical and economical reasons. Furthermore, centralized control designs are dependent upon the system structure and cannot handle structural changes. If new subsystems are added or removed, the controller for the overall system has to be redesigned.

Decentralized control approach arises as a consequence of the high order system dimensions, difficulties to interchange information between subsystems, the lack of computational resources if a centralized controller is required and the uncertainties due to parameter variations in large scale systems

In this thesis the recurrent high order neural networks applicability is verified and used as adaptive identifiers of large scale systems using only local information available; interconnection between subsystems are considered as disturbances and a discontinuous controller is implemented using the variable structure control theory. The developed algorithms are applied via simulations to several electromechanical systems and the applicability of such algorithms is verified for interconnected electromechanical systems

Acknowledgments

This thesis is dedicated to:

my family, for their unconditional love and support.

I want to express my gratitude to

Dr. Edgar Sanchez and Dr. Alexander Loukianov, for their time, knowledge, patience and directions to develop this dissertation.

Dr. Juan M. Ramirez, for the advices that help me out to understand several topics related with this dissertation.

Dra. Alma Y. Alanis, for her friendship and comments which helped to improve the content of this thesis.

CONACYT, Mexico, for granting the scholarship, which allow me to develop this dissertation.

Contents

Chapter 1

Introduction

1.1 Motivation

Many physical systems, such as electric power grids, computer and communication networks, networked dynamical systems, transportation systems and many others, are complex large-scale interconnected systems [17], [35]. To control such large scale systems, centralized control schemes are proposed in the literature assuming available global information for the overall system. While there are obvious theoretical advantages, control centralization is very difficult for a complex large scale system with interconnections due to technical and economic reasons [17]. Furthermore, centralized control designs are dependent upon the system structure and cannot handle structural changes. If subsystems are added or removed, the controller for the overall system should be redesigned.

Decentralized control for interconnected power systems has also attracted considerable attention of researchers in the field of complex and large-scale systems [6], [7], [14], [34]. We know that multi-area interconnected power systems have a complex structure. They exist in network forms; in some special cases, they can also exist in longitudinal, loop or radial structure.

Over the past three decades, the properties of linear interconnected systems have been widely studied [13], [19], [34]. By contrast, the control or modeling of interconnected nonlinear systems has not received the same attention. Due to physical

configuration and high dimensionality of interconnected systems, centralized control is neither economically feasible nor even necessary [2]. Because decentralized control schemes are free from difficulties due to complexity in design, debugging, data gathering, and storage requirements, they are preferable for interconnected systems than centralized ones. However, due to the existence of nonlinear interconnections, there are not many efficient methods to cope with the disturbances produced by the interconnection between subsystems.

Typical examples, where decentralized control approach can be applied, arises in different kind of industries, systems and processes. The process industry, such as the chemical one, include a broad range of large-scale processes: bulk petrochemicals, pulp and paper and cement are examples of them. Moreover there exist systems whose dynamical behavior changes according to unknown external disturbances or due to parameter variations. In a system of couple water reservoirs, for example, whose levels have to be controlled, effects, due to dynamical interactions between the reservoirs and uncertainties relative to human consumptions and inflow variations from the environment, need to be considered. In a multi-area power system, whose goal is to provide energy to many enterprisers and private consumers, there are dynamical variations due to changes in loads, new interconnections with other networks, changes in parameter due to saturation and operational conditions, etc. Numerous techniques and approaches are popular in industry in order to deal with large-scale systems, such as the relative gain array (RGA) [5] and partial relative gain (PRG) [15]. These procedures are developed to deal with multivariable linear plants; for nonlinear plants where there exist uncertainties, parameter variations and unmodelled dynamics, the mentioned techniques are difficult to apply. The aforementioned large-scale plants have one property in common: they are all complex collections of interacting components in which change often occurs as a resulting of not predictable processes. All these examples illustrate either the lack of centralized information, or the lack of a centralized computing facility. These facts motivate the design of decentralized controllers, using only local information while guaranteeing stability for the whole system.

1.2 Recurrent High Order Neural Networks

According to the structures of the neural networks, they can be classified as feed-forward neural networks (FFN) and recurrent neural networks (RNN) [9]. It is well known that a FFN is able to approximate any continuous function closely. However, the FFN is a static mapping. Without the aid of delays, FFN are unable to represent a dynamic mapping. In the two last decades, much research has been done on applications of FNN with delays to deal with dynamical problems; however, FFN require a large number of neurons to represent dynamical responses in the time domain [29]. On the other hand, RNN have superior capabilities than FNN, such as dynamics and the ability to store information for later use. Thus RNN is a dynamic mapping and demonstrates good control and identification performance in the presence of unmodelled dynamics [9]. Recently, research on RNN has been done on recurrent high order neural networks (RHONN). Additionally to the approximation properties of RNN, the RHONN structures have the capability to represent dynamic mappings in the state space form [4], [11], [22], [32]. Thus, RHONN allows the applicability of nonlinear control techniques designed in the state space approach [1], [3], [4], [11].

1.3 Block control and sliding modes

The variable structure control (VSC) strategy using sliding mode have been proven to be an excellent approach to control nonlinear dynamic systems [26], [36]. VSC offers attractive properties such as robustness to parameter variations, fast dynamics and the rejecting of external disturbances [36]. There are two basic steps to designing a VSC. The firs is the design of sliding control or equivalently the sliding surface. The second is the design of switching control. The system is reduced to normal or regular form before to start the designing. The electromechanical systems considered in this dissertation are already in this form.

1.4 Dissertation Structure

The present dissertation introduces a new approach for decentralized control theory: decentralized Recurrent High Order Neural Networks (RHONN) structures based on [21], which are able to identify the dynamical behavior of nonlinear subsystems with only local information and can deal with uncertainties in the absence of matching conditions, as has been discussed in [4]. VSC is used to obtain a robust control law, which guarantees tracking and rejects disturbances. The matching condition is not required due to the interconnection terms are considered external disturbances and they are embedded in the neural parameters; this allows to use only local information for the local controllers. Additionally, the use of reduced neural structures is presented in order to identify the dynamical model of power systems and the respective controllers based on such reduced models are designed. This work is organized as follows

In *Chapter 1*, the motivation for this dissertation is given, the state of the art on decentralized control is described. The block control technique and RHONN structures are described briefly.

In *Chapter 2*, the decentralized neural identifier and the class of subsystem considered is presented. The neural identifiers is designed considering the interconnection terms as external disturbances. A robust decentralized learning law is used for the local subsystems in order to avoid the drift parameter phenomenon.

In *Chapter 3*, the block control technique is explained. The block control algorithm is designed in a recursive manner. Each local subsystem is transformed in new coordinates in order to obtain the switching surface. The stability analysis for the local subsystems is detailed considering that interconnection terms are bounded but no necessary known. Hence, the closed loop for the whole system is guaranteed via Lyapunov analysis. The decentralized identification and control scheme developed is applied to a testbench large scale plant: the interconnected double inverted pendulum. Simulations results for regulation and tracking are presented.

In *Chapter 4*, a single machine infinite bus system application is developed. An $8th$

dynamical model for the power system and a reduced identifier is used. The sliding mode control based on the resulting reduced identifier is applied. The robustness of the scheme is tested via a short circuit fault.

In *Chapter 5*, two multimachine power systems are considered. The first one, is a two machine interconnected to an infinite bus system with a $3rd$ order dynamical model representation. The second multimachine power system is a 3-machine 9-bus interconnected via a transmission network. The 3 machine system is modeled as a $6th$ order dynamic structure and identified by a $3rd$ order reduced neural model. Both power systems are tested with a disturbance consisting of a short circuit fault.

Finally, *Chapter 6*, states conclusions and future work.

Chapter 2

Neural Network Identifier

In this chapter, we present the class of nonlinear systems to be considered in this dissertation and the decentralized recurrent neural network which is able to identify interconnected electromechanical plants. The respective convergence of the identification error is established on the basis of the Lyapunov approach [8], [22].

The considered large-scale system is constituted of nonlinear subsystems in the Nonlinear Block Controllable Form with Disturbance Term (NBC) [27] consisting of r blocks:

$$\begin{aligned}
\dot{\chi}_i^1 &= f_{i1}\left(\chi_i^1\right) + B_{i1}\left(\chi_i^1\right)\chi_i^2 + \Gamma_{i1k}\left(\bar{\chi}_k^1\right) \\
\dot{\chi}_i^2 &= f_{i2}\left(\chi_i^1, \chi_i^2\right) + B_{i2}\left(\chi_i^1, \chi_i^2\right)\chi_i^3 + \Gamma_{i2k}\left(\bar{\chi}_k^1, \bar{\chi}_k^2\right) \\
&\vdots \\
\dot{\chi}_i^q &= f_{iq}\left(\chi_i^1, \chi_i^2, \ldots, \chi_i^q\right) + B_{iq}\left(\chi_i^1, \chi_i^2, \ldots, \chi_i^q\right)\chi_i^r \\
&\quad + \Gamma_{iqk}\left(\bar{\chi}_k^1, \bar{\chi}_k^2, \ldots, \bar{\chi}_k^q\right), \quad q = 3, ..., r-1 \\
\dot{\chi}_i^r &= f_{ir}\left(\chi\right) + B_{ir}\left(\chi\right)u_i + \Gamma_{irk}\left(\bar{\chi}\right)
\end{aligned} \tag{2.1}$$

where $\chi = \left[\ \chi_i^{1T} \quad \chi_i^{2T} \quad \cdots \quad \chi_i^{rT}\ \right]^T$ $\chi_i^q \in R^{n_{iq}\times 1}$, $\bar{\chi}$ is the state vector of the k^{th} subsystem ($i = 1...N$, $1 \leq k < N$, $k \neq i$) and the rank of $B_{iq} = n_{iq}$, $\forall \chi_i^q \in D_{\chi_i^q} \subset R^{n_{iq}}$. The interconnection terms

$$
\begin{aligned}
\Gamma_{i1k} &= \sum_{k=1,k\neq i}^{N} \gamma_{i1k}\left(\bar{\chi}_k^1\right) \\
\Gamma_{i2k} &= \sum_{k=1,k\neq i}^{N} \gamma_{i2k}\left(\bar{\chi}_k^1, \bar{\chi}_k^2\right) \\
&\vdots \\
\Gamma_{iqk} &= \sum_{k=1,k\neq i}^{N} \gamma_{iqk}\left(\bar{\chi}_k^1, \bar{\chi}_k^2, \ldots, \bar{\chi}_k^q\right) \\
\Gamma_{irk} &= \sum_{k=1,k\neq i}^{N} \gamma_{irk}\left(\bar{\chi}\right)
\end{aligned}
\tag{2.2}
$$

reflect the interaction between the i^{th} and k^{th} subsystem; they are bounded by nonlinear functions γ_{irk} and enter the system as no matching condition disturbances, f_{ir} and B_{ir} are smooth and bounded functions, $f_{ir}(0) = 0$ and $B_i(0) = 0$. The integers $n_{i1} \leq n_{i2} \leq \ldots \leq n_{ir}$ defines the different subsystem structures, and $\sum_{q=1}^{r} n_{iq} = n_i$.

2.1 Decentralized Neural Network

For the large-scale plant, described by (2.1), we propose the following decentralized RHONN model, whose structure is similar to (2.1) and has also the nonlinear block

controllable form according to [27]:

$$
\begin{aligned}
\dot{x}_i^1 &= -A_{i1}x_i^1 + \sum_{p=1}^{L_{1p}} w_{i1p} \prod_{j\in I_{1p}} Z_{1p}^{d_{1j}(p)} + \sum_{m=L_{1p}+1}^{L'_{1p}} w'_{i1m}\Psi_{i1}\left(x_i^1\right) x_i^2 \\
\dot{x}_i^2 &= -A_{i2}x_i^2 + \sum_{p=1}^{L_{2p}} w_{i2p} \prod_{j\in I_{2p}} Z_{2p}^{d_{2j}(p)} + \sum_{m=L_{2p}+1}^{L'_{2p}} w'_{i2m}\Psi_{i2}\left(x_i^1, x_i^2\right) x_i^3 \qquad (2.3) \\
&\vdots \\
\dot{x}_i^q &= -A_{iq}x_i^q + \sum_{p=1}^{L_{qp}} w_{iqp} \prod_{j\in I_{qp}} Z_{qp}^{d_{qj}(p)} + \sum_{m=L_{qp}+1}^{L'_{qp}} w'_{iqm}\Psi_{iq}\left(x_i^1, x_i^2, ..., x_i^q\right) x_i^r \\
&\quad q = 3, ..., r-1 \\
\dot{x}_i^r &= -A_{ir}x + \sum_{p=1}^{L_{rp}} w_{irp} \prod_{j\in I_{rp}} Z_{rp}^{d_{rj}(p)} + \sum_{m=L_{rp}+1}^{L'_{rp}} w'_{irm}\Psi_{ir}\left(x\right)
\end{aligned}
$$

where $x = \left[\begin{array}{cccc} x_i^{1T} & x_i^{2T} & \cdots & x_i^{rT} \end{array}\right]^T$ is the i^{th} block neuron state with the same properties than (2.1), L_{qp} is the number of high order connections, L' is the number of fixed parameters w', which depends on the plant structure and are incorporated to the neural network model in order to obtain a block controllable structure, $\{I_{1p}, I_{2p}, ..., I_{rp}\}$ is a collection of no ordered subsets of $\{1_p, 2_p, ..., m+n\}$, A is a semi-definite positive matrix, w are the on-line adjustable weights of the neural network, d are no negative integers, Ψ is a nonlinear function of the state x and/or the input u, and Z_p is a vector defined as

$$
Z_p = \left[\begin{array}{c} s_i\left(x_i^1\right) \\ \vdots \\ s_i\left(x_i^r\right) \end{array}\right]
$$

with $s_i\left(\cdot\right)$ a smooth sigmoid function formulated as

$$
s_i\left(x\right) = \frac{\alpha_i}{1+\exp\left(-\beta_i x\right)} - \gamma_i
$$

where $s_i(\cdot) \in [-1, 1]$; α_i, β_i and γ_i are positive constants. If the following vector is introduced for the i^{th} subsystem

$$\rho_i(x_i, u_i) = \begin{bmatrix} \rho_{i,1} \\ \rho_{i,2} \\ \vdots \\ \rho_{i,L_p} \end{bmatrix} = \begin{bmatrix} \prod_{j \in Ii1} Z_1^{d_{1j}(i1)} \\ \prod_{j \in Ii2} Z_2^{d_{2j}(i2)} \\ \vdots \\ \prod_{j \in Iir} Z_r^{d_{rj}(ir)} \end{bmatrix} \tag{2.4}$$

then, system (2.3) can be rewritten as

$$\begin{aligned} \dot{x}_{ij} &= -a_{ij}x_{ij} + w_i^T \rho_i(x_i, u_i) + w_i'^T \psi_i(x, u)\, x_{j+1} \\ j &= 1, ..., r-1 \end{aligned} \tag{2.5}$$

In (2.5), the j^{th} state of each neuron for the i^{th} subsystem is characterized by x, and ψ denotes a nonlinear function of x or u which is selected according to the plant structure represented by the r blocks.

It is worth to point out that the design of decentralized neural network does not consider the interconnection terms. Although the neural identifier has a similar structure as (2.1)-(2.2), these interactions are considered as external disturbances and the identifier must be able to adapt its neural weights to compensate the influence of such external disturbances.

2.2 Decentralized On-Line Learning Law

The decentralized identification proposed is based only on local information available for each subsystem. Hence, the learning law is developed for the i^{th} subsystem as follows.

Based on the results presented in [21], we assume that there exists a decentralized RHONN which describes (2.1); thereby, the plant model can be described by

$$\dot{\chi}_i = -A_i \chi_i + w_i^{*T} \rho_i(\chi_i, u_i) + \nu_i(t) \tag{2.6}$$

where $w^* \in R^{L_{ir}}$ and the modeling error $\nu_i(t)$ is given by

$$\begin{aligned} \nu_i(t) &= f_i(\chi_i) + B_i(\chi_i)u_i + \Gamma_{i1k}(\bar{\chi}_k) \\ &\quad + A_i\chi_i - w_i^T\rho_i(\chi_i, u_i) \end{aligned} \tag{2.7}$$

The modeling error term $\nu_i(t)$ can be made arbitrary small selecting appropriately the number L of high order connections [22]. The optimal unknown weights vector w^* is defined as

$$w_i^* = \arg\min_{w_i} \left\{ \sup_{\chi_i, u_i} \left| f_i + B_i u_i + A_i\chi_i - w_i^T\rho_i \right| \right\}$$

Since each subsystem (2.1) can be written according to (2.6), two possible models for (2.5) can be used:

- Parallel model

$$\dot{x}_{ij} = -a_{ij}x_{ij} + w_i^T\rho_i(x_i, u_i) + w_i'^T\psi_i(x, u) \tag{2.8}$$

- Series-Parallel model

$$\dot{x}_{ij} = -a_{ij}x_{ij} + w_i^T\rho_i(\chi_i, u_i) + w_i'^T\psi_i(\chi, u) \tag{2.9}$$

We use the series-parallel model considering that, in the case of electromechanical plants included in this dissertation, it performs better than the parallel one.

A major concern when using adaptive schemes for control purposes is the stability of neural weights. The *parameter drift phenomenon*, which consist in the possibility that the RHONN synaptic parameters may drift to infinite, even if the identification error converges to zero, does it impossible to obtain parameter convergence.

To address such issues, we uses a robust updating weight law, which will be introduced in the next section, based on the following assumption, in order to guarantee the stability convergence for the proposed identification and control approach:

Assumption 1 *Systems (2.1) and (2.5) are input-to-state stables [11].*

tracking of a desired trajectory, defined in terms of the plant state χ_{ri}, by the nonlinear state χ_i formulated as (2.1), can be established as the following inequality

$$\|\chi_{ri} - \chi_i\| \leq \|x_i - \chi_i\| + \|\chi_{ri} - x_i\|, \quad i = 1, 2, 3, ..., N \tag{2.10}$$

where $\|\ \|$ stands for the Euclidian norm. We establish the following requirements for the neural network tracking and control solution [11]:

Requirement 1

$$lim_{t\to\infty}\|x_i - \chi_i\| \leq \zeta_i \tag{2.11}$$

with ζ_i a small positive constant.

Requirement 2

$$lim_{t\to\infty}\|\chi_{ri} - x_i\| = 0, \quad i = 1, 2, 3, ..., N \tag{2.12}$$

An on-line neural identifier based on (2.5) ensures (2.11), whereas (2.12) is guaranteed by a discontinuous controller based on the block control technique. Such control algorithm will be developed in the next chapter.

2.3 On-line Learning Law

In this subsection, an on-line updating weight law is developed considering the case where the modeling error term is zero, i.e., $\nu_i(t) = 0$. From (2.6), for the j^{th} state of the i^{th} subsystem, we establish

$$\begin{aligned} \dot{\chi}_{ij} &= -a_{ij}\chi_{ij} + w_{ij}^{*T}\rho_{ij}, \\ i &= 1, .., N, \\ j &= 1, ..., n_{iq} \end{aligned} \tag{2.13}$$

and considering (2.8) or (2.9) then

$$\begin{aligned} \dot{x}_{ij} &= -a_{ij}x_{ij} + w_{ij}^T\rho_{ij} \\ i &= 1,..,N, \\ j &= 1,...,n_{iq} \end{aligned} \tag{2.14}$$

where w_{ij} is the estimated of the unknown vector w_{ij}^*. In this case the state error $e_{ij} \triangleq x_{ij} - \chi_{ij}$ satisfies

$$\begin{aligned} \dot{e}_{ij} &= -a_{ij}e_{ij} + \phi_{ij}^T\rho_{ij} \\ i &= 1,..,N, \\ j &= 1,...,n_{iq} \end{aligned} \tag{2.15}$$

with $\phi_{ij} = w_{ij} - w_{ij}^*$. The following theorem establishes the main properties of the learning law which is able to on-line adjust the weights for neural network (2.14).

Theorem 1 *Consider the RHONN model given by (2.14) whose weights are adjusted according to*

$$\dot{w}_{ij}^i = -e_{ij}^i(\Xi_{ij}^i)^{-1}\rho_{ij}^i \tag{2.16}$$

where $(\Xi_{ij}^i)^{-1}$ *is a symmetric positive definite matrix, then for* $i = 1,...,N$ *and* $j = 1,...,n_{iq}$

(a) $e_{ij},\ \phi_{ij} \in \mathcal{L}_\infty$

(b) $lim_{t\to\infty} e_{ij}(t) = 0$

The respective proof and stability analysis is given in [32], [22].

2.4 Robust On-line Learning Law

For the case where the modelling error is not zero [32], the solutions of the differential equations (2.16) may become unbounded, even if the modelling error is bounded.

Therefore, the learning law (2.16) has to be modified in order to avoid the parameter drift problem. The learning laws given by (2.16) are modified as follows [32]

$$\dot{w}_{ij}^{i} = -(\Xi_{ij}^{i})^{-1} \left(e_{ij}\rho_{ij} - \sigma_{ij} w_{ij}\right) \tag{2.17}$$

where

$$\sigma_{ij}^{i} = \begin{cases} 0 & if \quad \|w_{ij}\| \leq M_{ij} \\ \left(\frac{\|w_{ij}\|}{M_{ij}}\right)^{q_{ij}} \sigma_{ij0} & if \quad M_{ij} < \|w_{ij}\| \leq 2M_{ij} \\ \sigma_{ij0} & if \quad \|w_{ij}\| > 2M_{ij} \end{cases}$$

with $q \geq 1$, σ_{ij0} and M_{ij} positive constants.

Chapter 3

Decentralized Block Control

Based on the large-scale system identified by the proposed subsystem neural identifier, we proceed to develop the respective control law. Stability of subsystems and global system is analyzed via Lyapunov approach. In order to test our developed decentralized identification and control scheme, we use an illustrative benchmark plant known as the two interconnected inverted pendulum. This example is a classical large-scale testbed for nonlinear decentralized control [3], [13], [19], [28], [35]. Simulation results are included, which illustrates the capabilities and performance of our approach.

3.1 Block Control Algorithm

A sliding surface and a discontinuous control law is designed for system (2.5) considering the state x_i^{q+1}, $q = 3, ..., r-1$ as a fictitious control vector for the block q. This procedure is described in the next steps [27].

Step 1 Assume that $n_{i1} = n_{i2}$ as discussed in [26], and define the vector error as

$$z_i^1 = x_i^1 - \delta_i \tag{3.1}$$

where δ_i is a smooth and bounded reference signal. The dynamics for (3.1) along the trajectories of (2.5) are

$$\begin{aligned} \dot{z}_i^1 &= -a_i x_i + w_i^T \rho_i(x_i, u_i) \\ &\quad + w_i'^T \psi_i(x, u) x_2 - \dot{\delta}_i \end{aligned} \tag{3.2}$$

If the fictitious control x_i^2 is selected as

$$\begin{aligned} x_i^2 &= \mu_i \left(-k_{i1} z_i^1 + z_i^2 + \dot{\delta}_i + a_i x_i - \eta_i \right) \\ \mu_i &= \left(w_i'^T \psi_i (x, u) \right)^{-1} \\ \eta_i &= w_i^T \rho_i (x_i, u_i) \end{aligned} \tag{3.3}$$

where k is a positive constant, then, the first block is transformed to the new coordinates z_i^1, z_i^2 as follows

$$\dot{z}_i^1 = -k_{i1} z_i^1 + z_i^2 \tag{3.4}$$

The vector z_i^2 is obtained using (3.3) as

$$\begin{aligned} z_i^2 &= -a_i x_i + w_i^T \rho_i (x_i, u_i) \\ &\quad + w_i'^T \psi_i (x, u) x_2 - \dot{\delta}_i + k_{i1} z_i^1 \end{aligned} \tag{3.5}$$

$$z_i^2 \triangleq \alpha_i^1 (x_{i1}, x_{i2}) \tag{3.6}$$

Step 2 Taking the derivative of (3.5), we obtain

$$\dot{z}_i^2 = \frac{\partial \alpha_i^1}{\partial x_{i1}} \dot{x}_{i1} + \frac{\partial \alpha_i^1}{\partial x_{i2}} \dot{x}_{i2} - \ddot{\delta}_i \tag{3.7}$$

The fictitious control for (3.7) is x_i^3 and the procedure continues for the remainder blocks until the true control u_i is obtained in the r^{th} block as

$$\dot{z}_i^r = f_{ir} - \xi_{ir} u_i \tag{3.8}$$

where the rank of $\xi_{ir} = n_{ir}$ and f_{ir} is a bounded function. The discontinuous control action is applied as

$$u_i = U_{i0} sign (z_i^r) \tag{3.9}$$

3.2 Stability Analysis for the Proposed Controller

The closed loop Stability of subsystems and global system is analyzed via the Lyapunov approach in the following theorem.

Theorem 2 *Let define*

$$B_i = \{f_{ir} \in R^{n_{ir}} \mid \|f_{ir}\| < \epsilon_i\} \tag{3.10}$$

as a ball of radius ϵ. *Setting* U_{i0} *in (3.9) as*

$$U_{0i} > \frac{(\epsilon_i + \alpha_{i0})}{\xi_{ir}} \tag{3.11}$$

with α_{i0} *a positive constant. Let consider the candidate Lyapunov function*

$$v_i = \frac{1}{2} z_{ir}^T z_{ir} \tag{3.12}$$

whose derivative along the trajectories of (3.8) are obtained as

$$\dot{v}_i = z_{ir}^T \left(f_{ir} - \xi_{ir} U_{i0} sign\left(z_{ir}\right)\right) \tag{3.13}$$

Taking into account the following identities

$$z^T sign\left(z\right) = \|z\|_1 \geq \|z\|_2$$

and substituting them in (3.13), we obtain

$$\begin{aligned} \dot{v}_i &\leq \|z_{ir}\| \|f_{ir}\| - \xi_{ir} U_{0i} \|z_{ir}\| \\ \dot{v}_i &\leq -\|z_{ir}\| \left(-\|f_{ir}\| + \xi_{ir} U_{i0}\right) \end{aligned} \tag{3.14}$$

If (3.10) holds and using (3.11) in (3.14), the derivative of the Lyapunov function is simplified as

$$\dot{v}_i \leq -\alpha_{i0} \|z_{ir}\| \tag{3.15}$$

Consequently, the closed loop asymptotic stability is guarantee for (3.8) and the sliding motion occurs on the manifold $z_i^r = 0$ *in a finite time, then the tracking error (3.1) will tends asymptotically to zero in accordance with (3.4). Moreover, the composite Lyapunov function candidate for the large-scale system* $V = \sum_{i=1}^{N} v_i$ *whose derivative*

$$\dot{V} \leq -\sum_{i=1}^{N} \alpha_{i0} \|z_{ir}\| \tag{3.16}$$

is negative defined, guarantees the stability for the global interconnected system if ***Requirement 2*** *holds and (3.10) is fulfilled.*

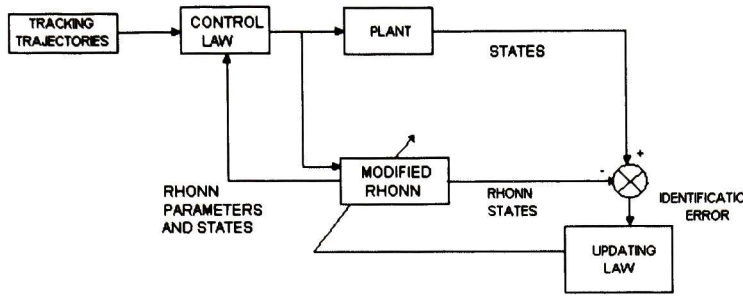

Figure 3.1: Identification and control scheme

Additionally, according to **Theorem 1** the identification errors are bounded. Then, considering (2.10) and (2.12), it is possible to establish the bound of the tracking error $\|\chi_{ri} - x_i\|$ for the whole interconnected system. The closed loop identification and control scheme developed is shown in Fig. 3.1.

3.3 Interconnected Double Inverted Pendulum

This section is devoted to test the decentralized scheme developed using a benchmark plant. Applicability of decentralized identification and control algorithms is illustrated via simulations; additionally, regulation and tracking of nonlinear reference signals is depicted using this decentralized testbed system.

3.3.1 Plant description

Each pendulum is positioned by a torque input u_i applied to a servomotor at its base. It is assumed that, for the i^{th} controller $(i = 1, 2)$, the only available measurements are χ_{i1} and $\dot{\chi}_{i1}$ (angular position and angular rate) corresponding to the respective pendulum.

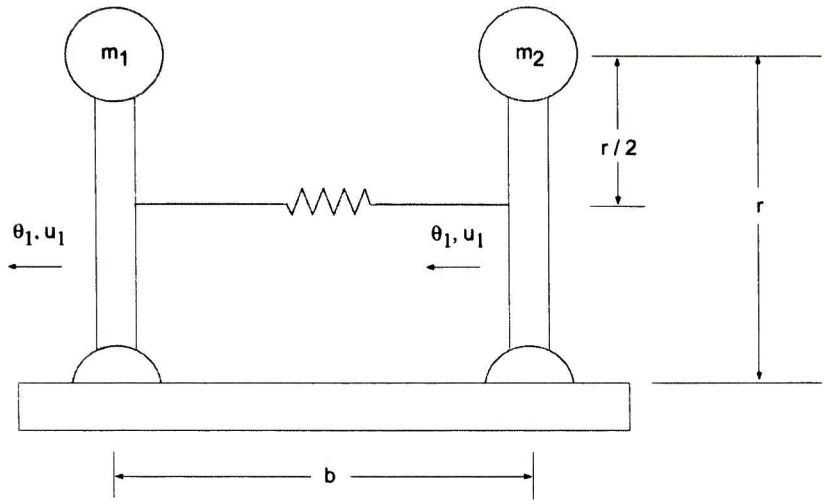

Figure 3.2: Double inverted pendulum

The equations which describe the motion of each pendulum are defined as

$$\dot{\chi}_{i1} = \chi_{i2} \tag{3.17}$$

$$\dot{\chi}_{i2} = \left(\frac{m_i g r}{J_i} - \frac{k r^2}{4 J_i}\right) \sin(\chi_{i1}) + \frac{k r}{2 J_i}(l - b) + \frac{u_i}{J_i} + \frac{k r^2}{4 J_i}\gamma_{i2} \tag{3.18}$$

$$\gamma_{i2} = \begin{cases} \sin(\chi_{21}) & if \quad i = 1 \\ \sin(\chi_{11}) & if \quad i = 2 \end{cases} \tag{3.19}$$

$$i = 1, 2$$

where χ_{i1} is the angular displacement of the pendulums from the vertical and χ_{i2} is the angular speed. The parameters values are indicated in Table 3.1 and Fig. 3.2 displays a scheme of the system.

For the plant dynamics (3.17)-(3.19), we propose the decentralized neural network

Table 3.1: Double interconnected inverted pendulum parameters

Description	Parameter	Value	Unit
Pendulum end mass 1	m_1	2	Kg
Pendulum end mass 2	m_2	2.5	Kg
Moment of inertia 1	J_1	0.5	$Kg \cdot m^2$
Moment of inertia 2	J_2	0.625	$Kg \cdot m^2$
Spring constant	k	100	N/m
Pendulum height	r	0.5	m
Natural length of the spring	l	0.5	m
Gravitational acceleration	g	9.81	m/s^2
Distance between pendulum hinges	b	0.4	m

identifiers, according to the series-parallel model (2.9) as

$$\begin{aligned} \dot{x}_{i1} &= x_{i2} \\ \dot{x}_{i2} &= -a_{i2}x_{i2} + w_{i21}s_i(\chi_{i1}) + w_{i22}s_i(\chi_{i2}) + \frac{u_i}{J_i} \\ i &= 1,2 \end{aligned} \tag{3.20}$$

The block diagram implementing (2.4) is shown in Fig. 3.3. In this diagram, the entries to the sigmoid blocks are the plant states available, χ_{i1} and χ_{i2}, according to the series-parallel model described in (2.9).

The goal is to track desired reference signals; this tracking is achieved by designing a control law based on the sliding mode technique as described in section 3.1.

Considering the reference signal as δ_i, for $i = 1, 2$, the tracking error is given by

$$z_{i1} = x_{i1} - \delta_i \tag{3.21}$$

whose dynamics are obtained using (3.20) as

$$\dot{z}_{i1} = x_{i2} - \dot{\delta}_i \tag{3.22}$$

Introducing new dynamics for (3.22) as

$$\dot{z}_{i1} = -k_{i1}z_{i1} + z_{i2} \tag{3.23}$$

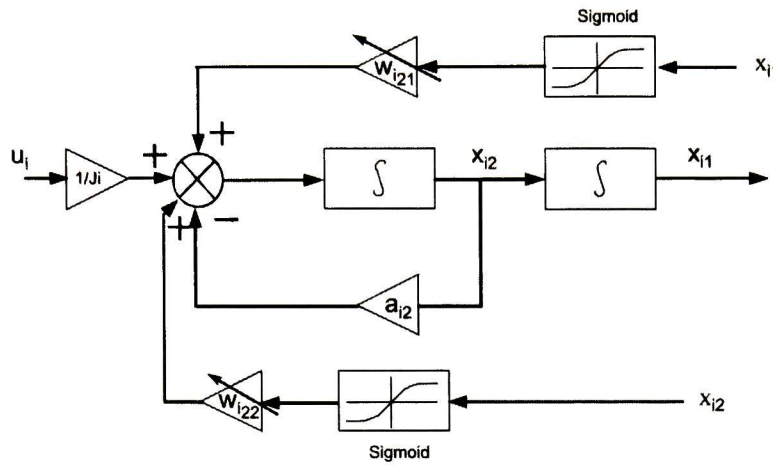

Figure 3.3: Time-domain block diagram for the proposed structure.

then, the dynamics for new variables z_{i2} are obtained

$$\dot{z}_{i2} = f_{i2} + \frac{1}{J_i} u_i \tag{3.24}$$

where

$$\begin{aligned} f_{i2} &= -a_{i2}x_{i2} + w_{i21}s_i(\chi_{i1}) + w_{i22}s_i(\chi_{i2}) \\ &\quad -\ddot{\delta}_i - k_{i1}^2 z_{i1} + k_{i1} z_{i2} \end{aligned} \tag{3.25}$$

Hence, the control action is proposed, for each pendulum ($i = 1, 2$), as

$$u_i = -U_{i0} sign(z_{i2}), \quad U_{i0} > J_i f_{i2} \tag{3.26}$$

3.3.2 Simulation results

This section presents the respective simulation results for the interconnected double inverted pendulum. First the regulation case is displayed; afterward, the tracking one is presented.

Regulation is depicted in Fig. 3.4, which includes a 10 $N - m$ torque disturbance applied at 3 sec. Fig. 3.5 and Fig. 3.6 shows the applied decentralized discontinuous

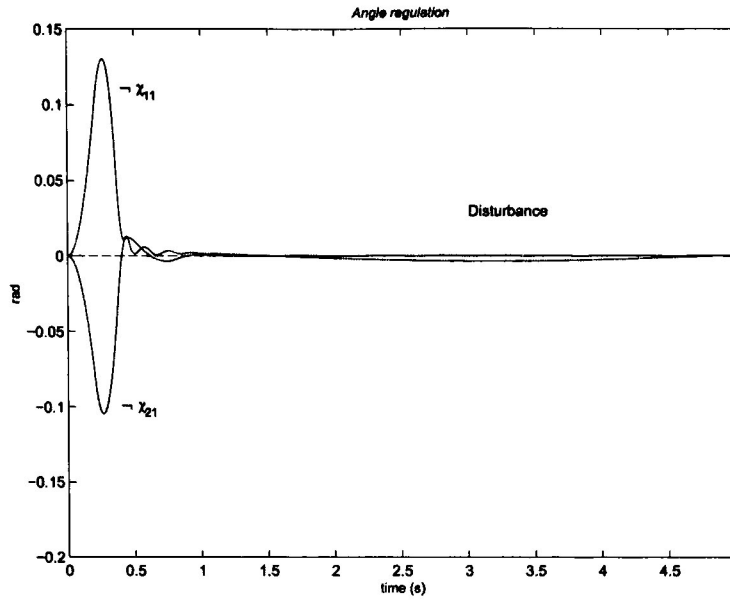

Figure 3.4: Regulation

control action. The identification error behavior is shown in Fig. 3.7 and Fig. 3.8 for pendulum 1 and pendulum 2 respectively.

The decentralized identification and control scheme proposed is able to track reference signals δ_i. The tested reference signals include sinusoidal ones, whose dynamical characteristics is useful to illustrate the proposed approach performance. In Fig. 3.9 a reference $\delta_1 = \delta_2 = 0.1\sin(t)$ for both pendulums is tracked.

More complex tracking capabilities are illustrated by Fig. 3.10 and Fig. 3.11.

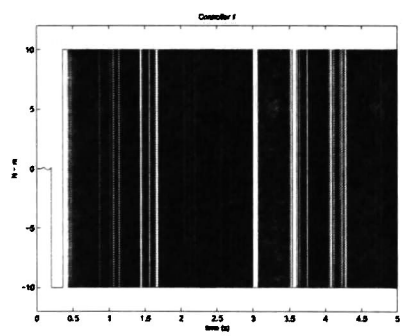

Figure 3.5: Control action 1

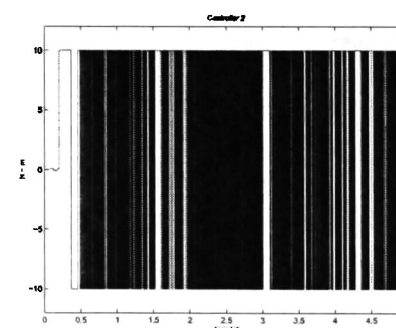

Figure 3.6: Control action 2

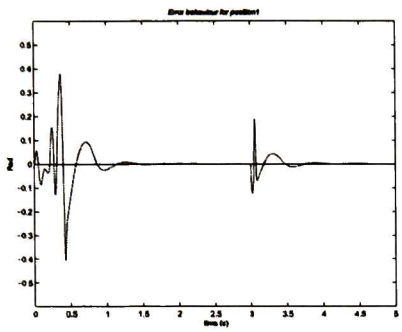

Figure 3.7: Error behavior 1

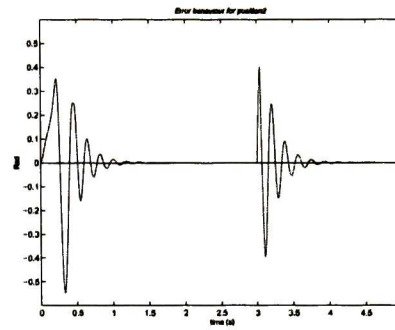

Figure 3.8: Error behavior 2

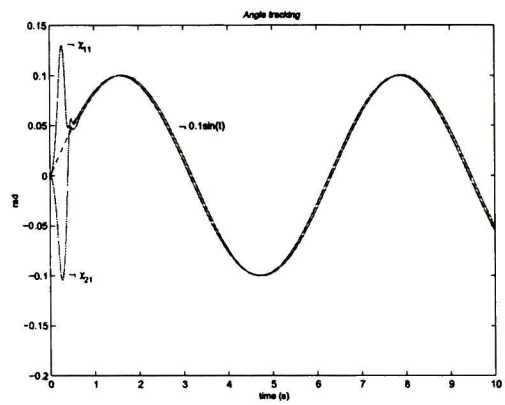

Figure 3.9: Tracking for a sine reference

Fig. 3.10 shows the state χ_{11} tracking a sinus signal, whereas χ_{21} tracks a cosine signal. In Fig. 3.11 one pendulum is forced to stay at a fixed position, whereas the other one tracks a sinusoidal signal.

It is worth to point out that all the methods found in literature are applied for stabilization; our approach is able, additionally to regulation, to track reference signals as showed in this section. The sliding mode technique generates a very high frequency signal only when the sliding surface is reached. Moreover, the power stage could be based on the well known IGBT technology, which is adequate for discontinuous control signals.

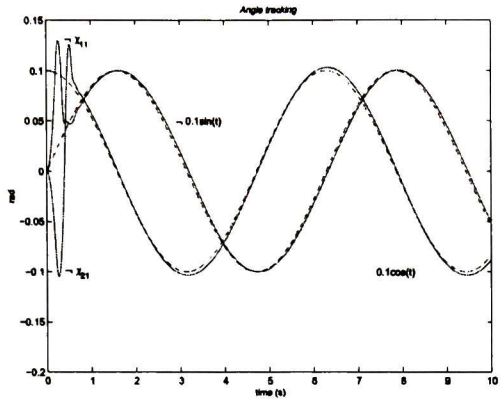

Figure 3.10: Tracking for a sine and cosine reference signals

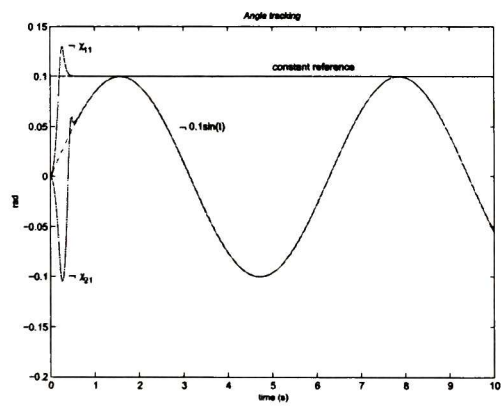

Figure 3.11: Tracking for a constant and sine reference signals

Chapter 4

Single machine infinite bus system application

Motivated by the results obtained in the interconnected double inverted pendulum application presented in Chapter 3, in this chapter, we consider to test out a neuronal control scheme based on a reduced neural model to a single machine infinite bus system (SMIB). A complete SMIB dynamical model is used and a reduced neural identifier is proposed in order to obtain a control law based on this reduced order neural identifier. This chapter presents a design which addresses the on-line identification and control trajectory tracking based on the 3rd order neural model of the power system and the application of the resulting controller to the 8th order plant [25]. The goal of this chapter is related to the applicability of a reduced order neural identifier to high order nonlinear plant such a synchronous generator. The identification and control scheme developed allows to obtain a control law using the reduced neural identifier parameters, whose mathematical representation is less complex than the full order mathematical model of SMIB. Additionally the block control technique allows to use the robust sliding mode control as illustrated via simulations.

4.1 Mathematical Model

This section describes the required mathematical models.

4.1.1 Full Order Mathematical Model

The complete model of the single machine infinite-bus system consists of electrical and mechanical dynamics and load constraints. The electrical dynamics comprising the stator and rotor damping windings, employing the currents as the state variables, can be modeled as

$$L \begin{bmatrix} \frac{di_s}{dt} \\ \frac{di_r}{dt} \end{bmatrix} = - \begin{bmatrix} G_1 & G_2 \\ G_3 & G_4 \end{bmatrix} \begin{bmatrix} i_s \\ i_r \end{bmatrix} + \begin{bmatrix} V_s \\ V_r \end{bmatrix} \tag{4.1}$$

where

$$L = \begin{bmatrix} -L_d & 0 & L_{md} & 0 & L_{md} & 0 \\ 0 & -L_q & 0 & L_{mq} & 0 & L_{mq} \\ -L_{md} & 0 & L_f & 0 & L_{md} & 0 \\ 0 & -L_{mq} & 0 & L_g & 0 & L_{mq} \\ -L_{md} & 0 & L_{md} & 0 & L_{kd} & 0 \\ 0 & -L_{mq} & 0 & L_{mq} & 0 & L_{kq} \end{bmatrix}$$

$$G_1 = \begin{bmatrix} -R_S & \omega L_q & 0 \\ -\omega L_d & -R_S & \omega L_{md} \\ 0 & 0 & R_f \end{bmatrix} \quad G_2 = \begin{bmatrix} -\omega L_{mq} & 0 & -\omega L_{mq} \\ 0 & \omega L_{mq} & 0 \\ 0 & 0 & 0 \end{bmatrix}$$

$$G_3 = \begin{bmatrix} 0 & 0 & 0 \\ 0 & 0 & 0 \\ 0 & 0 & 0 \end{bmatrix} \quad G_4 = \begin{bmatrix} R_g & 0 & 0 \\ 0 & R_{kd} & 0 \\ 0 & 0 & R_{kq} \end{bmatrix}$$

with $i_s = \begin{bmatrix} i_d & i_q \end{bmatrix}^T, i_r = \begin{bmatrix} i_f & i_g & i_{kd} & i_{kq} \end{bmatrix}^T \; V_s = \begin{bmatrix} V_d & V_q \end{bmatrix}^T \; V_r = \begin{bmatrix} V_f & 0 & 0 & 0 \end{bmatrix}^T$

i_d and i_q are the direct-axis and quadrature-axis stator currents, in per unit (p.u);

i_f is the field current, in p.u;

i_{kd}, i_{kq}, and i_g are the direct-axis and quadrature-axis damper windings currents, in p.u;

ω is the angular velocity, in rad/s;

V_d and V_q are the direct and quadrature-axis terminal voltages, in p.u;

V_f is the excitation control input, in p.u;

R_s and R_f are the stator and field resistances, in p.u;

R_g, R_{kd} and R_{kq} are the damper windings resistances, in p.u;

L_d and L_q are the direct and quadrature-axis self-inductances, in p.u;

L_f is the rotor self-inductance, in p.u;

L_{kd} and L_{kq} are the direct and quadrature-axis damper windings self-inductances, in p.u;

L_{md} and L_{mq} are the direct and quadrature-axis magnetizing inductances, in p.u.

It is well known that fluxes are less sensitivity with respect to parameter variations than currents; hence, it is more suitable to represent the electrical dynamics in terms of the stator currents i_s and the rotor fluxes ϕ_r, where $\phi_r = \left[\begin{array}{cccc} \psi_f & \psi_g & \psi_{kd} & \psi_q \end{array} \right]^T$, is in p.u. Such model is obtained from (4.1) using the following transformation between fluxes and currents:

$$\left[\begin{array}{c} i_s \\ \phi_r \end{array} \right] = T \left[\begin{array}{c} i_s \\ i_r \end{array} \right] \tag{4.2}$$

where

$$T = \left[\begin{array}{cccccc} 1 & 0 & 0 & 0 & 0 & 0 \\ 0 & 1 & 0 & 0 & 0 & 0 \\ -L_{md} & 0 & L_f & 0 & L_{md} & 0 \\ 0 & -L_{mq} & 0 & L_g & 0 & L_{mq} \\ -L_{md} & 0 & L_{md} & 0 & L_{kd} & 0 \\ 0 & -L_{mq} & 0 & L_{mq} & 0 & L_{kq} \end{array} \right]$$

System (4.1) is transformed to the form

$$\left[\begin{array}{c} \frac{di_s}{dt} \\ \frac{d\phi_r}{dt} \end{array} \right] = A_e(\omega) \left[\begin{array}{c} i_s \\ \phi_r \end{array} \right] + B_e \left[\begin{array}{c} V_s \\ V_r \end{array} \right] \tag{4.3}$$

with $A_e(\omega) = -TL^{-1}G(\omega)T^{-1}$ and $B_e = TL^{-1}$ The complete mathematical description includes the swing equation [2]

$$\frac{d\delta}{dt} = \omega - \omega_s \tag{4.4}$$

$$\frac{d\omega}{dt} = \frac{\omega_s}{2H}(T_m - T_e) \tag{4.5}$$

where δ, in p.u, is the power angle of the generator; ω_s is the rated synchronous speed, in rad/s; H is the inertia constant, in sec; T_m is the mechanical torque applied to the shaft, in p.u; and T_e is the electrical torque, in p.u, expressed in terms of the currents as follows

$$T_e = (L_q - L_d)\, i_d i_q + L_{md} i_q\, (i_f + i_{kd}) - L_{mq} i_d\, (i_g + i_{kq}) \tag{4.6}$$

The mechanical torque T_m is assumed to be a slowly varying function of time as follows

$$\dot{T}_m = 0$$

The equilibrium equation for the external network is written as

$$V_s = \frac{L_e}{\omega_s}\frac{di_s}{dt} + R_L\,(\omega)\, i_s + V^{\infty} Y \tag{4.7}$$

where $R_L\,(\omega) = \begin{bmatrix} R_e & -\omega\frac{L_e}{\omega_s} \\ \omega\frac{L_e}{\omega_s} & R_e \end{bmatrix}$ and $Y = \begin{bmatrix} \cos\delta \\ \sin\delta \end{bmatrix}$ V^{∞} is the value of the infinite bus voltage; L_e and R_e are the transformer plus transmission line resistance and inductance. Parameter values of (4.1)-(4.7) are expressed in p.u.

If we select the following state variables

$$\begin{array}{llll} \chi_1 = \delta, & \chi_2 = \omega, & \chi_3 = \psi_f, & \chi_4 = \psi_g, \\ \chi_5 = \psi_{kd}, & \chi_6 = \psi_{kq}, & \chi_7 = i_d, & \chi_8 = i_q, \end{array}$$

then (4.1)-(4.7) can be represented by

$$\begin{aligned} \dot{\chi}^1 &= \chi^2 - \omega_s \\ \dot{\chi}^2 &= a_{26}(\begin{bmatrix} -a_{21}\chi_8 & -a_{22}\chi_7 \end{bmatrix} \chi^3 + \begin{bmatrix} -a_{23}\chi_8 & -a_{24}\chi_7 \end{bmatrix} \chi^4 - a_{25}\chi_7\chi_8 + T_m) \\ \dot{\chi}^3 &= A_{31}\chi^3 + A_{32}\chi^4 + A_{33}\chi^5 + B_1 v_f \\ \dot{\chi}^4 &= A_{41}\chi^3 + A_{42}\chi^4 + A_{43}\chi^5 \\ \dot{\chi}^5 &= A_{51}\chi^3 + A_{52}\chi^4 + A_{53}\chi^5 + A_{54}J\chi^3 + A_{55}J\chi^2\chi^4 + A_{56}J\chi^2\chi^5 + A_{57}Y + B_2 v_f \end{aligned} \tag{4.8}$$

where

$\chi^1 = [\chi_1]$, $\chi^2 = [\chi_2]$, $\chi^3 = \begin{bmatrix} \chi_3 & \chi_4 \end{bmatrix}^T$ $\chi^4 = \begin{bmatrix} \chi_5 & \chi_6 \end{bmatrix}^T$ $\chi^5 = \begin{bmatrix} \chi_7 & \chi_8 \end{bmatrix}^T$

$A_{31} = \begin{bmatrix} a_{31} & 0 \\ 0 & a_{41} \end{bmatrix}$ $A_{32} = \begin{bmatrix} a_{32} & 0 \\ 0 & a_{42} \end{bmatrix}$ $A_{33} = \begin{bmatrix} a_{33} & 0 \\ 0 & a_{43} \end{bmatrix}$ $A_{41} = \begin{bmatrix} a_{51} & 0 \\ 0 & a_{61} \end{bmatrix}$

$$A_{42} = \begin{bmatrix} a_{52} & 0 \\ 0 & a_{62} \end{bmatrix} \quad A_{43} = \begin{bmatrix} a_{53} & 0 \\ 0 & a_{63} \end{bmatrix} \quad A_{51} = \begin{bmatrix} a_{71} & 0 \\ 0 & a_{81} \end{bmatrix} \quad A_{52} = \begin{bmatrix} a_{72} & 0 \\ 0 & a_{82} \end{bmatrix},$$
$$A_{53} = \begin{bmatrix} a_{73} & 0 \\ 0 & a_{83} \end{bmatrix} \quad A_{54} = \begin{bmatrix} a_{74} & 0 \\ 0 & a_{84} \end{bmatrix} \quad A_{55} = \begin{bmatrix} a_{75} & 0 \\ 0 & a_{85} \end{bmatrix} \quad A_{56} = \begin{bmatrix} a_{76} & 0 \\ 0 & a_{86} \end{bmatrix}$$
$$A_{57} = \begin{bmatrix} a_{77} & 0 \\ 0 & a_{87} \end{bmatrix} \quad B_1 = \begin{bmatrix} a_{34} \\ 0 \end{bmatrix} \quad B_2 = \begin{bmatrix} a_{78} \\ 0 \end{bmatrix} \quad J = \begin{bmatrix} 0 & 1 \\ 1 & 0 \end{bmatrix}$$

v_f is the control input to be designed.

4.1.2 Reduced mathematical model

The machine model considered is the flux decay model (one axis model) given in [2] and [24]; exciters and governors are not included in this model. The reduced dynamics of a single synchronous generator is described by the following equations in state variable form

$$\begin{aligned} \dot{\chi}_1 &= \chi_2 \\ \dot{\chi}_2 &= -b_1\chi_3 \sin(\chi_1) - b_2\chi_2 + P \\ \dot{\chi}_3 &= b_3 \cos(\chi_1) - b_4\chi_3 + E + u \end{aligned} \tag{4.9}$$

where χ_1 is the load angle, χ_2 is the shaft speed deviation from the synchronous speed, χ_3 is the quadrature axis internal voltage, $P = \frac{\omega_s P_m}{2H}$, $E = \frac{E_{fd}}{T'_{d0}}$ and u is a supplementary signal added to the field voltage, as a control input. The coefficients b_i, $i = 1, ..., 4$ are positive [12].

4.2 Neural Model for Synchronous Generators

Based on the reduced order model (4.9) and the series-parallel structure (2.9), a reduced neural identifier structure is proposed as

$$\begin{aligned} \dot{x}_1 &= -a_1 x_1 + \xi_1 \\ \dot{x}_2 &= -a_2 x_2 + w_{21} S(x_2) + w_{22} S(x_1) S(x_3) + \xi_2 \\ \dot{x}_3 &= -a_3 x_3 + w_{31} S(x_1) + w_{32} S(x_3) + \xi_3 \end{aligned} \tag{4.10}$$

In accordance with (2.9), the structure of (4.10) consists of parameters to be adjusted such as w_{21}, w_{22} and w_{31}, w_{32}; the fixed terms are given by

$$\begin{aligned} \xi_1 &= a_1 x_1 + x_2 - \omega_s \\ \xi_2 &= P \\ \xi_3 &= E + u \end{aligned} \tag{4.11}$$

The adjustable neural weights of (4.10) are updating using the robust on-line learning law (2.17) as established in chapter 2.

4.3 Control Algorithm

The objective is to force angle χ_1 to track a desired reference signal χ_r and at the same time rejecting external disturbances. Employing the block control technique [27] and using χ_r as a constant reference value to be tracked, let define the error signal as

$$z_1 = x_1 - \chi_r. \tag{4.12}$$

The dynamics for (4.12) can be obtained from (4.10) and (4.11) as

$$\dot{z}_1 = x_2 - \omega_s. \tag{4.13}$$

Using $x_2 = -k_1 z_1 + z_2 + \omega_s$, (4.13) is modified to

$$\dot{z}_1 = -k_1 z_1 + z_2, \tag{4.14}$$

with $\dot{z}_2$ given by

$$\dot{z}_2 = -a_2 x_2 + w_{21} s(x_1)\, s(x_3) + w_{22} s(x_1)\, s(x_3) + k_1 (x_2 - \omega_s) + P. \tag{4.15}$$

In the next step, the switching surface z_3 is introduced in (4.15)

$$\dot{z}_2 = -k_2 z_2 + z_3, \tag{4.16}$$

where $k_1, k_2 > 0$. The switching function z_3 is obtained using (4.15) and (4.16) as

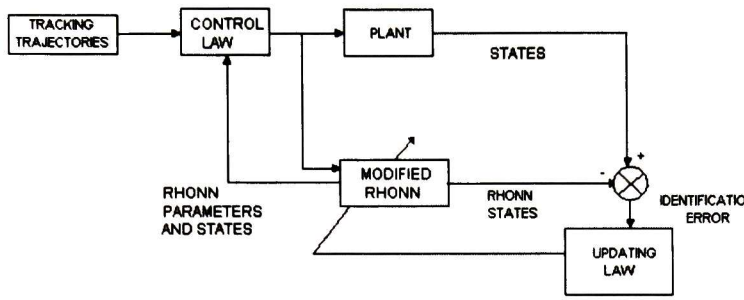

Figure 4.1: Identification and control scheme

follows

$$z_3 = -a_2 x_2 + w_{21} s(x_1)\, s(x_3) + w_{22} s(x_1)\, s(x_3) + k_1 (x_2 - \omega_s) + P + k_2 z_2. \quad (4.17)$$

It is clear that if we select the following sliding manifold

$$z_3 = 0, \quad (4.18)$$

then the motion on this manifold will be described by linear system (4.14) and (4.16) with the desired dynamics. To guarantee the sliding mode in the manifold (4.18), the motion projection on subspace z_1, z_2 is derived as [36]

$$\dot{z}_3 = \eta + w_{22} s(x_1)\, s'(x_3)\, u, \quad (4.19)$$

where $\eta = \frac{\partial z}{\partial x_1}\dot{x}_1 + \frac{\partial z}{\partial x_2}\dot{x}_2 + \frac{\partial z}{\partial r}\dot{r}$, $s'(x) = \frac{\partial s(x)}{\partial x}\dot{x}$, with $r = \begin{bmatrix} \chi_r & \omega_s \end{bmatrix}^T$ Then, taking into account the bound $|u| \leq U_0$, $U_0 > 0$, the discontinuous control law is defined as

$$u = -U_0 sign\left(w_{22} s(x_1)\, s'(x_3)\right) sign(z_3), \quad (4.20)$$

The stability condition of the origin $z_3 = 0$ for the closed-loop system (4.19), (4.20) is

$$\dot{z}_3 = \eta - U_0 \left| w_{22} s(x_1)\, s'(x_3) \right| sign(z_3), \quad (4.21)$$

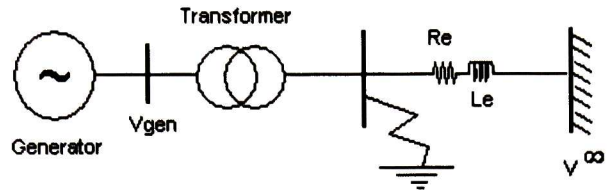

Figure 4.2: Single machine-infinite bus system

If the following inequality is satisfied

$$|\eta| < U_0 \left| w_{22} s(x_1) s'(x_3) \right|, \tag{4.22}$$

a sliding mode motion occurs on the manifold (4.18) in a finite time, then the tracking error z_1 will tends asymptotically to zero in accordance with (4.14). This motion is invariant with respect to generator parameters variations and external disturbances. Fig. 4.1 illustrates the proposed identification and block control scheme.

4.4 Simulations

The proposed identification and control scheme is applied on the complete 8^{th} order model (4.8) of the generator connected to an infinite bus through a transmission line. Fig. 4.2 depicts the single-machine infinite bus system. The parameters of the synchronous machine and transmission system (4.8) are indicated in Table 4.1, which are in p.u except when indicated.

The reference angle χ_r to be tracked is equal to 1.3314. The parameters for the neural identifier are $a_2 = 1$, $a_3 = 2$, $\alpha_2 = \alpha_3 = 2$, $\beta_2 = 20$, $\beta_3 = 20$, $\varepsilon = 0.01$, $\Gamma_2^{-1} = 800$, $\Gamma_3^{-1} = 0.2$. The identification and control stages are indicated as follows

Stage 1: The open loop system is identified on-line by the neural network from $t_0 = 0$ to $t_i = 20$ s;

Parameter	Value (pu)	Parameter	Value (pu)
a_{21}	0.4851	a_{71}	26.0460
a_{22}	-0.1379	a_{72}	-28.7592
a_{23}	0.4667	a_{73}	-42.2029
a_{24}	-0.8	a_{74}	-0.2602
a_{25}	0.02	a_{75}	-1.5094
a_{26}	$\frac{\omega_s}{2H}$	a_{76}	1.0870
a_{31}	-0.7116	a_{77}	-711.3040
a_{32}	0.6456	a_{78}	345.0824
a_{33}	-0.1107	a_{81}	13.6301
a_{34}	ω_s	a_{82}	-20.1334
a_{41}	-2.776	a_{83}	-46.7986
a_{42}	2.576	a_{84}	0.8821
a_{43}	-0.3220	a_{85}	0.8485
a_{51}	30.6122	a_{86}	-0.9663
a_{52}	-33.333	a_{87}	-685.4384
a_{53}	-5	H	3.525 sec
a_{61}	9.849	T_m	0.9463
a_{62}	-14.286	L_e	0.1
a_{63}	-7.1429	Re	0.5

Table 4.1: Parameter values for generator.

Stage 2: The control law is incepted at $t = t_i$;

Stage 3: A fault occurs at $t_{f1} = 40sec$;

Stage 4: The fault is removed by opening the breakers of the faulted line at $t_{f2} = 40.15sec$;

Stage 5: The system is in a postfault state. This system goes back to healthy operation (stage 1).

The identification and control sequence for χ is showed in Fig. 4.4, whereas Fig. 4.5 displays a zoom in for χ.

The short circuit fault occurs at $t_{f1} = 40$ sec and is cleared at $t_{f2} = 40.15$ sec. The lapse $t_{f2} - t_{f1}$ is called the critical clearing time.

Fig. 4.3 shows the performance of the identification and control scheme for ω. The

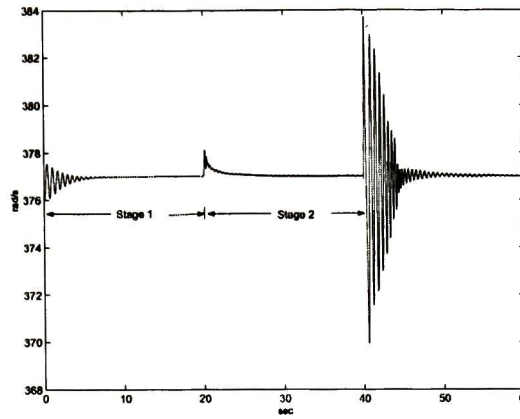

Figure 4.3: Angle speed time evolution

weights remains bounded all the time (Fig. 4.6). Fig. 4.7 depicts the discontinuous control signal.

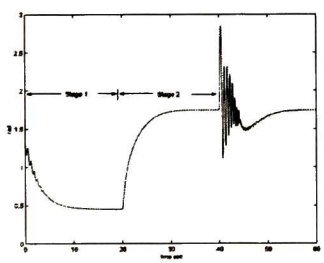

Figure 4.4: Angle time evolution

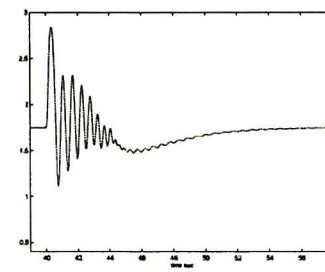

Figure 4.5: Zoom in for angle in short circuit stage

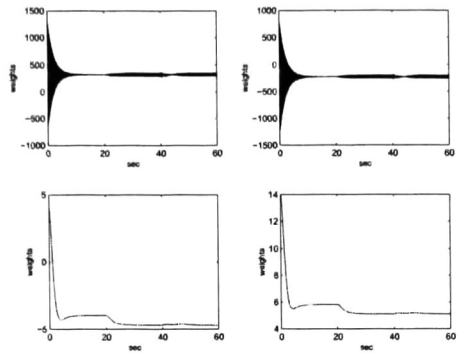

Figure 4.6: Neural identifier weights

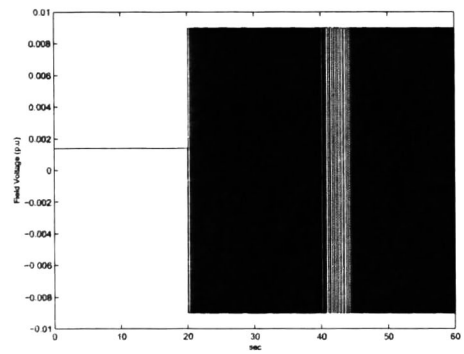

Figure 4.7: Discontinuous control action

Chapter 5

Interconnected Power System Applications

This chapter extends the proposed adaptive neuronal identification and control scheme to the case with two machines interconnected to an infinite bus and with a 3-machine power system. A decentralized RHONN structure, and the respective learning law, are proposed in order to approximate on-line the dynamical behavior of each nonlinear subsystem. The control law, which is able to force the system to track the desired reference signals, is designed using the well known variable structure theory. The stability of the whole system is analyzed via the Lyapunov methodology. The applicability of proposed decentralized identification and control algorithm is illustrated via simulations to stabilize a electric power system in presence of external disturbance. In the case of the 3-machine power system, a reduced neural identifier is used to approximate the dynamical behavior of the multimachine system.

5.1 Power System Dynamical Model

The large-scale power system considered is constituted by n generators interconnected through a transmission network, whose dynamics are modelled by (see [14] and refe-

rences within for details)

$$\begin{aligned} \dot{\delta}_i &= \omega_i \\ \dot{\omega}_i &= -\frac{D_i}{2H_i}\omega_i - \frac{\omega_0}{2H_i}\Delta P_{ei} \\ \Delta\dot{P}_{ei} &= -\frac{1}{T'_{d0i}}\Delta P_{ei} + \frac{1}{T'_{d0i}}v_{fi} + \gamma_i(\delta,\omega) \end{aligned} \tag{5.1}$$

where

$$\Delta P_{ei} = P_{ei} - P_{mi0} \tag{5.2}$$

$$\begin{aligned} \gamma_i(\delta,\omega) &= E'_{qi}\sum_{j=1}^{n}\dot{E}'_{qj}B_{ij}\sin(\delta_i-\delta_j) \\ &\quad -E'_{qi}\sum_{j=1}^{n}E'_{qj}B_{ij}\cos(\delta_i-\delta_j)\omega_j \end{aligned} \tag{5.3}$$

δ_i is the angle of the ith machine relative to the synchronous angle of the system, ω_i is the synchronous speed of the ith generator, P_{ei} is the electrical power, ω_0 is the synchronous machine speed, D_i is the damping constant, H_i is the inertia constant, E'_{qi} is the quadrature axis component of the voltage, B_{ij} are the ith row and jth column element of the nodal susceptance matrix at the internal nodes after eliminating all physical buses, v_{fi} is the control input and P_{mi0} is a constant.

The interconnection term γ_i bound is established considering that the internal voltages E' are always constrained taking into account physical considerations [14], [18]. Moreover, the excitation voltage may raise by up to 5 times of the E_{qi} when there is no load in the system, then

$$\begin{aligned} \left|E'_{qi}E'_{qj}B_{ij}\right| &\leq |p_{ei}|_{\max} \\ \left|\dot{E}'_{qj}\right| &\leq \left|\frac{1}{T'_{d0i}}\left(v_{fi}-E'_{qj}\right)\right|_{\max} \\ &\leq 4|E_{qj}|_{\max}\frac{1}{\left|T'_{d0j}\right|_{\min}} \end{aligned} \tag{5.4}$$

as explained in [18].

Considering (5.4), it is also established that

$$\gamma_i(\delta,\omega) \leq \sum_{j=1}^{n}\left(\gamma_{i1j}\left|\sin(\delta_j)\right| + \gamma_{i2}\left|\omega_j\right|\right) \tag{5.5}$$

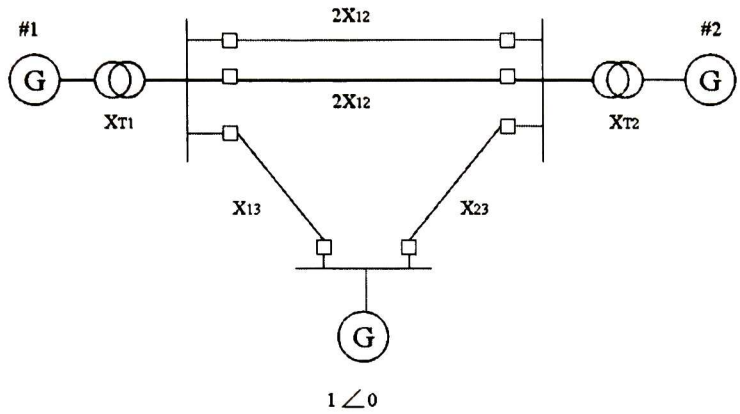

Figure 5.1: A two machines infinite bus power system

with

$$\gamma_{i1j} = \begin{cases} \sum_{j=1,j\neq 1}^{n} \frac{4p_{1ij}}{|T'_{d0j}|_{\min}} |p_{ei}|_{\max} & when \quad j = i \\ \frac{4p_{1ij}}{|T'_{d0j}|_{\min}} |p_{ei}|_{\max} & when \quad j \neq i \end{cases} \tag{5.6}$$

$$\gamma_{i2} = p_{2ij} |Q_{ei}|_{\max} \tag{5.7}$$

p_{1ij} and p_{2ij} are constants with values either 1 or 0.[1]

5.2 Interconnected Power System Example

In this section, the proposed decentralized scheme is applied using a two-generator infinite bus power system which is portrayed in Fig. 5.1. The plant parameters are listed in Table 5.1.

If we select the following state variables $\delta_i = \chi_{i1}$, $\omega_i = \chi_{i2}$ and $\Delta P_{ei} = \chi_{i3}$; then,

[1]when they are zero, it means that the jth subsystem is not connected with the ith subsystem

Table 5.1: System parameters

Parameter	Generator #1	Generator #2
x_d (pu)	1.863	2.36
x'_d (pu)	0.257	0.319
x_T (pu)	0.129	0.11
x_{ad} (pu)	1.712	1.712
T'_{d0} (pu)	6.9	7.96
H (s)	4	5.1
D (pu)	5	3
x_{12} (pu)	0.55	0.55
x_{13} (pu)	0.53	0.53
x_{23} (pu)	0.6	0.6
ω_0 (rad/s)	314.159	314.159

(5.1) can be represented as

$$\begin{aligned} \dot{\chi}_{i1} &= \chi_{i2} \\ \dot{\chi}_{i2} &= -\frac{D_i}{2H_i}\chi_{i2} - \frac{\omega_o}{2H_i}\chi_{i3} \\ \chi_{i3} &= -\frac{1}{T'_{d0i}}\chi_{i3} + \frac{1}{T'_{d0i}}v_{fi} + \gamma_i\left(\chi_{i1}, \chi_{i2}\right) \end{aligned} \tag{5.8}$$

5.2.1 Decentralized neural model identification and controller design

The following decentralized neural network identifiers are proposed for the plant dynamics (5.8)

$$\begin{aligned} \dot{x}_{i1} &= x_{i2} \\ \dot{x}_{i2} &= -a_{i2}x_{i2} + w_{i21}s_i^5\left(\chi_{i2}\right) + \frac{\omega_o}{2H_i}\left(p_{mi0} - \chi_{i3}\right) \\ \dot{x}_{i3} &= -a_{i3}x_{i3} + w_{i31}s_i^4\left(\chi_{i1}\right) + w_{i32}s_i^4\left(\chi_{i2}\right) \\ &\quad + w_{i33}s_i^4\left(\chi_{i3}\right) + \frac{1}{T'_{d0i}}\left(p_{mi0} + v_{fi}\right) \\ i &= 1, 2 \end{aligned} \tag{5.9}$$

The goal is to track desired reference signals δ_i; this tracking is achieved by designing a control law based on the sliding mode technique. Consider the constant reference

signal as δ_i, for $i = 1, 2$, then the tracking error is given by

$$\begin{aligned} z_{i1} &= x_{i1} - \delta_i \\ z_{i2} &= x_{i2} \end{aligned} \tag{5.10}$$

whose dynamics are obtained, using (5.9), as

$$\dot{z}_{i1} = x_{i2} \tag{5.11}$$

$$\dot{z}_{i2} = -a_{i2}x_{i2} + w_{i21}s_i^5(\chi_{i2}) + \frac{\omega_o}{2H_i}(p_{mi0} - \chi_{i3}) \tag{5.12}$$

$$\dot{z}_{i2} \triangleq \alpha_{i2}(x_i, \chi_i) \tag{5.13}$$

Introducing new dynamics for (5.12) as

$$\dot{z}_{i2} = -k_{i1}z_{i1} - k_{i2}z_{i2} + z_{i3} \tag{5.14}$$

using (5.12), the dynamics for the new variable z_{i3} is obtained as

$$\dot{z}_{i3} = f_{i3} - c_i v_{fi} \tag{5.15}$$

where $f_{i3} = \frac{\partial \alpha_{i2}}{\partial x_i}\dot{x}_i + \frac{\partial \alpha_{i2}}{\partial \chi_i}\dot{\chi}_i$ and $c_i = \frac{\omega_o}{2T'_{d0i}H_i}$.

Then, the control action proposed for each generator ($i = 1, 2$) is

$$v_{fi} = -U_{i0}sign(z_{i3}) \tag{5.16}$$

$$U_{0i} = 10 \tag{5.17}$$

5.2.2 Simulations

This section presents the respective simulation results. The simulated sequence is as follows

Stage 1: The open loop system is identified on-line by the neural network for time $0 \leq t < 0.2\ s$;

Stage 2: The control law is incepted in $t \geq 0.2\ s$;

Stage 3: A fault arises at $t = 15\ s$;

Stage 4: The fault is removed by opening the breakers of the faulted line at $t = 15.15\ s$;

Stage 5: The system is in a postfault state. This system goes back to healthy operation (stage 1).

Fig. 5.2 displays the angle time evolution for generator 1 for a reference signal $\delta_1 = 1.061 rad$. Fig. 5.3 shows the angle time evolution for generator 2, with $\delta_2 = 1.058$ rad. The robustness of the control action is tested via a short circuit fault, which is incepted at stage 3 and it is cleared at $t = 15.15$ seconds. Fig. 5.6 and Fig. 5.7 display the relative speed for both generators.

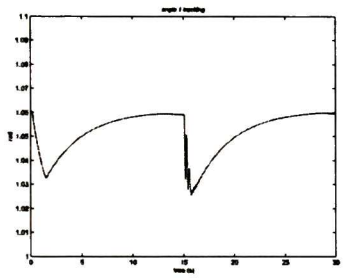

Figure 5.2: Angle 1 time evolution

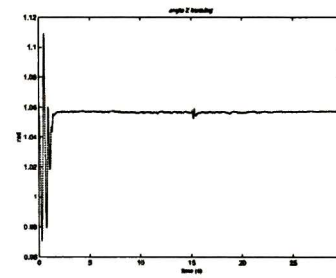

Figure 5.3: Angle 2 time evolution

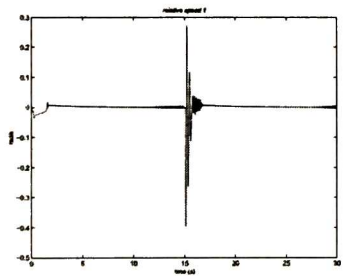

Figure 5.4: Speed 1 time evolution

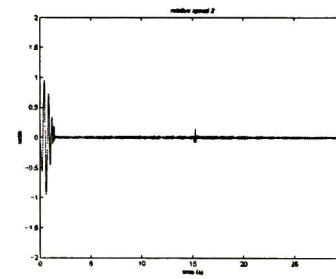

Figure 5.5: speed 2 time evolution

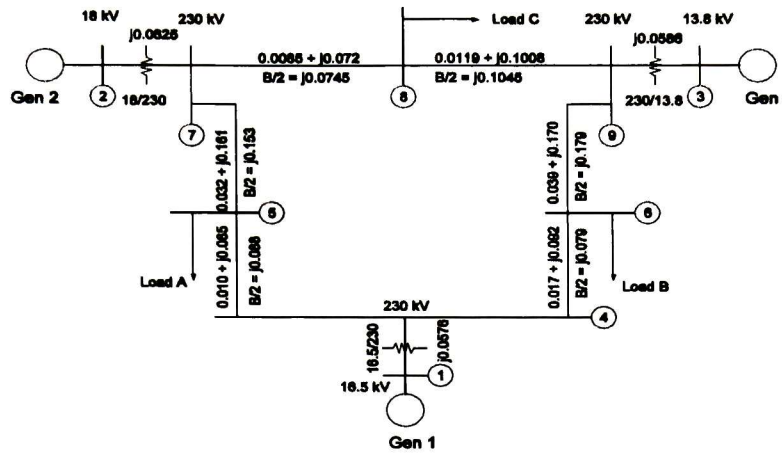

Figure 5.6: WSCC 3-machine 9-bus power system

5.3 Multimachine Power System

In this section, the proposed decentralized identification and control scheme is tested with the Western System Coordinating Council (WSCC) 3-machine, 9-bus system [30], [2]. The power system configuration is depicted in Fig. 5.6.

5.3.1 Mathematical model

The differential and algebraic equations which represent the *ith* generator dynamics and power flow constraints respectively are given by

$$
\begin{aligned}
\dot{\chi}_{1i} &= \chi_{2i} - \omega_s \\
\dot{\chi}_{2i} &= (\frac{\omega_s}{2H_i})(T_{mi} - (\psi_{di} I_{qi} - \psi_{qi} I_{di})) \\
\dot{\chi}_{3i} &= (\frac{1}{T'_{d0i}})(-\chi_{3i} - (X_{di} - X'di)[I_{di} - \frac{X'_{di} - X''_{di}}{(X'_{di} - X_{lsi})^2}(\chi_{5i} + (X'_{di} - X_{lsi})I_{di})] + E_{fdi}) \\
\dot{\chi}_{4i} &= (\frac{1}{T'_{q0i}})(-\chi_{4i} + (X_{qi} - X'_{qi})[I_{qi} - \frac{X'_{qi} - X''_{qi}}{(X'_{qi} - X_{lsi})^2}(\chi_{6i} + (X'_{qi} - X_{lsi})I_{qi} + E'_{di})]) \\
\dot{\chi}_{5i} &= (\frac{1}{T''_{d0i}})(-\chi_{5i} + \chi_{3i} - (X'_{di} - X_{lsi})I_{di}) \\
\dot{\chi}_{6i} &= (\frac{1}{T''_{q0i}})(-\chi_{6i} - \chi_{4i} - (X'_{qi} - X_{lsi})I_{qi}) \\
\psi_{di} &= -X''_{di} I_{di} + \frac{X''_{di} - X_{lsi}}{X'_{di} - X_{lsi}}\chi_{3i} + \frac{X'_{di} - X''_{di}}{X'_{di} - X_{lsi}}\chi_{5i} \\
\psi_{qi} &= -X''_{qi} I_{qi} - \frac{X''_{di} - X_{lsi}}{X'_{qi} - X_{lsi}}\chi_{4i} + \frac{X'_{qi} - X''_{qi}}{X'_{qi} - X_{lsi}}\chi_{6i}
\end{aligned}
\tag{5.18}
$$

$$
\begin{aligned}
0 &= P_i - V_i \sum_{j=1}^{n} V_j Y_{ij} \cos(\theta_i - \theta_j - \phi ij) \\
0 &= Q_i - V_i \sum_{j=1}^{n} V_j Y_{ij} \sin(\theta_i - \theta_j - \phi ij)
\end{aligned}
\tag{5.19}
$$

with currents I_{di} and I_{qi} satisfying the following equations

$$
\begin{aligned}
V_i \sin(\delta_i - \theta_i) - X_{qi} I_{qi} &= 0 \\
V_i \cos(\delta_i - \theta_i) + X'_{di} I_{di} - E'_{qi} &= 0 \\
i &= 1, 2, ...N.
\end{aligned}
\tag{5.20}
$$

where N is the number of generators, n is the number of buses, χ_{1i} is the power angle of the ith generator in rad, χ_{2i} is the rotating speed of the ith generator in rad/s, χ_{3i} is the q-axis internal voltage of the ith generator in p.u., χ_{4i} is the d-axis internal voltage of the ith generator in p.u., χ_{5i} is the $1d$-axis flux linkage of the ith generator in p.u., χ_{6i} is the $2q$-axis flux linkage of the ith generator in p.u., E_{fdi} is the excitation

control input, ψ_{di} and ψ_{qi} are the d-axis flux linkage and q-axis flux linkage of the ith generator in p.u. respectively; ω_s is the synchronous rotor speed in rad/s, P_i and Q_i is the injected active and reactive power at bus i in p.u., $V_i\angle\theta_i$ is the voltage at bus i and $Y_{ij}\angle\phi_{ij}$ is the admittance between bus i and bus j.

The algebraic equation constraints (5.19) and (5.20) can be manipulated to express currents I_{qi}, I_{di} as a function on the states (5.18). The voltages and injected currents at the generator buses are related by the expression

$$\bar{V} = Z\bar{I} \tag{5.21}$$

where $\bar{V} = [V_1, ..., V_n]^T$ and $\bar{I} = [I_1, ..., I_n]^T$ $Z = R + jX$ is a nxn matrix of the network equivalent impedance. Using the following equations which represents the dynamic circuit of the synchronous generator [33]

$$\bar{I} = (I_d + jI_q)e^j(\delta - \frac{\pi}{2}) \tag{5.22}$$

$$\bar{V} = [(X_qI_q - R_sI_d) + j(\chi_3 - X'_dI_d - R_sI_q)]e^j(\delta - \frac{\pi}{2}) \tag{5.23}$$

we can express (5.21) in term of the states as follows

$$\begin{aligned}
\chi_{qi}\cos(\delta_i) &= \sum_{j=1}^{n}[R_{ij}\sin(\delta_j) + (A_{ij} + X_{ij})\cos(\delta_j)]I_{dj} + [-(B_{ij} + X_{ij})\sin(\delta_{ij}) + R_{ij}\cos(\delta_j)]I_{qj} \\
\chi_{qi}\sin(\delta_i) &= \sum_{j=1}^{n}[(A_{ij} + X_{ij})\sin(\delta_j) - R_{ij}\cos(\delta_j)]I_{dj} + [R_{ij}\sin(\delta_j) + (B_{ij} + X_{ij})\cos(\delta_j)]I_{qj}
\end{aligned} \tag{5.24}$$

where R_{ij} and X_{ij} are parameter of the electrical network, A and B are defined as $A = diag[X'_{d1}, ..., X'_{dn}]$ and $B = diag[X_{q1}, ..., X_{qn}]$

5.3.2 Reduced neural identifier

A $3rd$ order neural model is used to identify the dynamics of (5.18). The decentralized neural identifier is proposed considering only angle, angle speed and q-axis internal

voltage of the ith generator. The recurrent high order neural identifier proposed is

$$\begin{aligned} \dot{x}_{1i} &= x_{2i} - w'_{i1} \\ \dot{x}_{2i} &= -a_{2i}x_{2i} + w_{2i}\rho_{2i} - w'_{2i}x_{3i} \\ \dot{x}_{3i} &= -a_{3i}x_{3i} + w_{3i}\rho_{3i} + w'_{3i}E_{fdi} \end{aligned} \tag{5.25}$$

where $w'_{i1} = \omega_s$, $w'_{2i} = (\frac{\omega_s}{2H_i})(\frac{X''_{di}-X_{lsi}}{X'_{di}-X_{lsi}})$, and $w'_{3i} = \frac{1}{T'_{d0i}}$ are the fixed parameters of the ith generator. It is worth to notice that in the reduced neural identifier (5.25), the interactions of the multimachine system are not explicitly included. Since I_{di} and I_{qi} can be expressed as linear combinations of χ_{qi}, together with the bounded parameters of the network in terms of the $\sin(\delta_i)$ and $\cos(\delta_i)$, then currents in (5.24) can be expressed by

$$\begin{aligned} I_{di} &= \sum_{j=1}^{n} \phi_{ij}(\bar{\delta})\chi_{qi} \\ I_{di} &= \sum_{j=1}^{n} \lambda_{ij}(\bar{\delta})\chi_{qi} \end{aligned} \tag{5.26}$$

with ϕ_{ij} and λ_{ij} defined as parameters of the electrical network (5.24), $\bar{\delta} = [\delta_1, ..., \delta_n]^T$ denote all of the rotor angles.

The linear combination of bounded variables remains bounded. Hence the bound for currents I_{di} and I_{qi} can be expressed as

$$\begin{aligned} |I_{di}| &\leq \sum_{j=1}^{n} \Phi_{ij}|\chi_{dj}| \\ |I_{qi}| &\leq \sum_{j=1}^{n} \Lambda_{ij}|\chi_{qj}| \end{aligned} \tag{5.27}$$

where Φ_{ij} and Λ_{ij} are the bounds of ϕ_{ij} and λ_{ij} respectively [14].

5.3.3 Controller design

Considering the ith subsystem, let define

$$z_{1i} = x_{1i} - \delta_{ri} \tag{5.28}$$

where δ_{ri} is the reference signal for the desired stable operation condition of the *ith* machine. The dynamic of (5.28) along the trajectory of (5.25) are

$$\dot{z}_{1i} = x_{2i} - \omega_s \tag{5.29}$$

Defining new dynamics for (5.29) as

$$\dot{z}_{1i} = -k_{1i} z_{1i} + z_{2i} \tag{5.30}$$

then, z_{i2} is obtained using (5.29) and (5.30)

$$z_{2i} = x_{2i} - \omega_s + k_{1i} z_{1i} \tag{5.31}$$

Taking the derivatives of z_{2i} along the trajectory of (5.25)

$$\dot{z}_{2i} = -a_{2i} x_{2i} + w_{2i} \rho_{2i} - w'_{2i} x_{3i} + k_{1i} \dot{z}_{1i} \tag{5.32}$$

a new dynamics for z_{2i} is defined as

$$\dot{z}_{2i} = -k_{2i} z_{2i} + z_{3i} \tag{5.33}$$

Then z_{3i} can be obtained using (5.32) and (5.33)

$$z_{3i} = -a_{2i} x_{2i} + w_{2i} \rho_{2i} - w'_{2i} x_{3i} + k_{1i} \dot{z}_{1i} + k_{2i} z_{2i} \tag{5.34}$$

The true control E_{fdi}, is obtaining with the derivative of (5.34) along trajectory of (5.25). If we select the following sliding manifold

$$z_{3i} = 0 \tag{5.35}$$

then the motion of this manifold will be described by linear system (5.30) and (5.33) with the desired dynamics. To guarantee a sliding mode in the manifold (5.35), the motion projection on subspace z_{1i}, z_{2i} is derived as

$$\dot{z_{3i}} = \bar{f} + U_{0i} E_{fdi} \tag{5.36}$$

where $\bar{f} = \frac{\partial z_i}{\partial x_i} \dot{x}_i$ and U_{0i} is a constant.

Then, the control action proposed for each generator ($i = 1, 2, 3$) is

$$E_{fdi} = U_{0i} sign\,(z_{3i}) \tag{5.37}$$

Table 5.2: Parameters of the generators

Parameter	Generator #1	Generator #2	Generator #3
H (sec)	23.64	6.4	3.01
T_m (pu)	0.716	1.63	0.85
T'_{d0} (sec)	8.9600	6.0000	5.8900
T''_{d0} (sec)	0.2000	0.3000	0.4000
T'_{q0} (sec)	0.3100	0.5350	0.6000
T''_{q0} (sec)	0.2000	0.3000	0.4000
X_d (pu)	0.146	0.8958	1.3125
X'_d (pu)	0.0608	0.1198	0.1813
X''_d (pu)	0.0200	0.0500	0.0800
X_q (pu)	0.0969	0.8645	1.2578
X'_q (pu)	0.0969	0.1969	0.2500
X''_q (pu)	0.0200	0.0500	0.0800
X_{ls} (pu)	0.0336	0.0521	0.0742

5.3.4 Simulations

In this section we present the simulation results obtained with the applications of the decentralized identification and control scheme to the WSCC power system. In order to simulate the performance of our decentralized scheme, the following data is required [2]

1. A load-flow study of the pre-transient network to calculate the mechanical power of the generators and to calculate the initial conditions values of voltages and angles of all generators. This data is shown in Table 5.4 and Table 5.3.

2. The inertia constant H, the reactance, the transmission network impedance for the initial network conditions for all generators, which is shown in Table 5.2 and 5.5.

3. The type and location of disturbance as well as the fault clearing time, these are explained in the simulation description.

The simulation is conducted following the stages

Table 5.3: Initial conditions of the generators

State	Generator #1	Generator #2	Generator #3
$\chi_1(rad)$	0.0625	1.0664	0.9460
$\chi_2(rad/s)$	377	377	377
$\chi_3(pu)$	1.056	0.788	0.768
$\chi_4(pu)$	0.000	0.622	0.624
$\chi_5(pu)$	1.0478	0.7007	0.7078
$\chi_6(pu)$	-0.0425	-0.7568	-0.7328

Table 5.4: Load-flow of the WSCC 3-machine, 9-bus system

Bus #	Type	Voltage (pu)	P_{gen} (pu)	G_{gen} (pu)	P_{load} (pu)	Q_{load} (pu)
1	Swing	1.04	0.716	0.27		
2	P-V	$1.025\angle 9.3$	1.63	0.067		
3	P-V	$1.025\angle 4.7$	0.85	-0.109		
4	P-Q	$1.026\angle -2.2$				
5	P-Q	$0.996\angle -4.0$			1.25	0.5
6	P-Q	$1.013\angle -3.7$			0.9	0.3
7	P-Q	$1.026\angle 3.7$				
8	P-Q	$1.016\angle 0.7$			1.0	0.35
9	P-Q	$1.032\angle 2.0$				

Table 5.5: Parameters of the transmission lines

Bus i	Bus j	R_{ij}	X_{ij}	G_{ij}	B_{ij}
1	4	0.0000	0.1184	0.0000	−8.4459
2	7	0.0000	0.1823	0.0000	−5.4855
3	9	0.0000	0.2399	0.0000	−4.1684
4	5	0.0100	0.0850	1.3652	−11.6041
4	6	0.0170	0.0920	1.9422	−10.5107
5	7	0.0320	0.1610	1.1876	−5.9751
6	9	0.0390	0.1700	1.2820	−5.5882
7	8	0.0085	0.0720	1.6171	−13.6980
8	9	0.0119	0.1008	1.1551	−9.7843
5	0	0.0000	0.0000	1.2610	−0.2634
6	0	0.0000	0.0000	0.8777	−0.0346
8	0	0.0000	0.0000	0.9690	−0.1601
4	0	0.0000	0.0000	0.0000	0.1670
7	0	0.0000	0.0000	0.0000	0.2275
9	0	0.0000	0.0000	0.0000	0.2835

Stage 1: The open loop system is identified on-line by the neural network from $t_0 = 0$ to $t_i = 2\ s$;

Stage 2: The control law is incepted at $t = 2sec$;

Stage 3: A fault occurs at $t_{f1} = 10sec$ near bus 7;

Stage 4: The fault is removed by opening the breakers of the faulted line at $t_{f2} = 10.15sec$;

Stage 5: The system is in a postfault state. This system goes back to healthy operation (stage 1).

In Fig. 5.7, Fig. 5.8 and Fig. 5.9 the time evolution for angles is shown. The Fig. 5.10, Fig. 5.11 and Fig. 5.12 illustrates the rotor speed behavior.

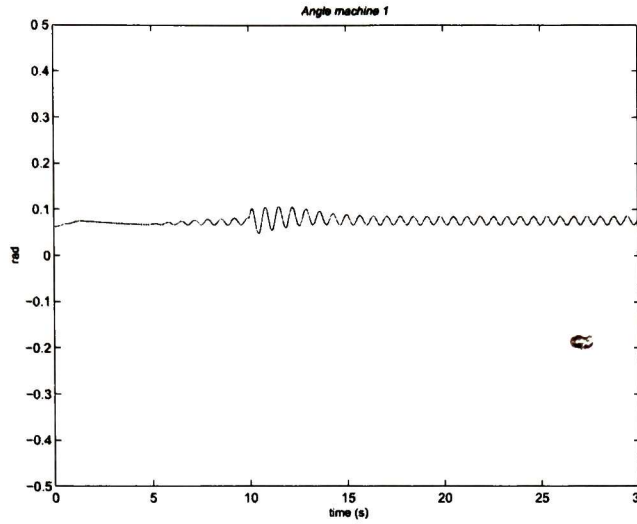

Figure 5.7: Rotor angle time evolution for machine 1

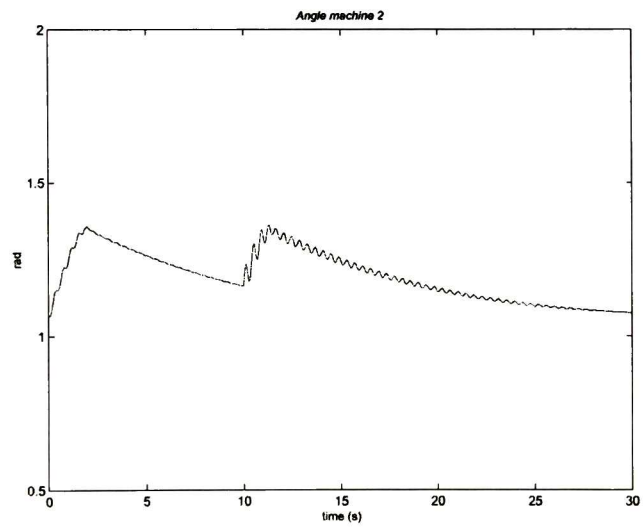

Figure 5.8: Rotor angle time evolution for machine 2

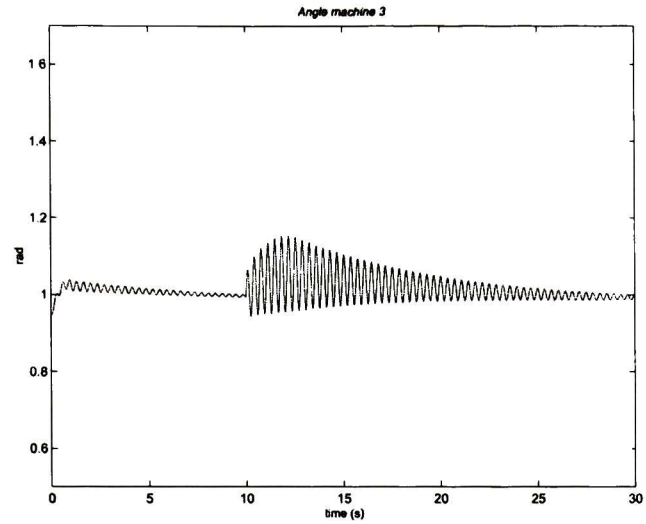

Figure 5.9: Rotor angle time evolution for machine 3

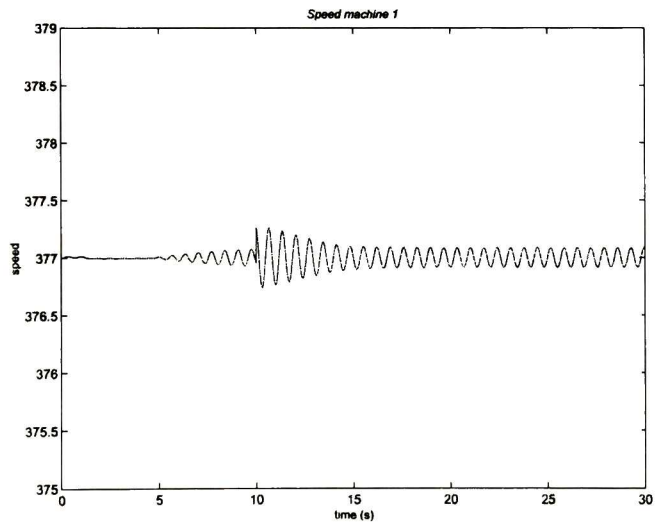

Figure 5.10: Rotor speed time evolution for machine 1

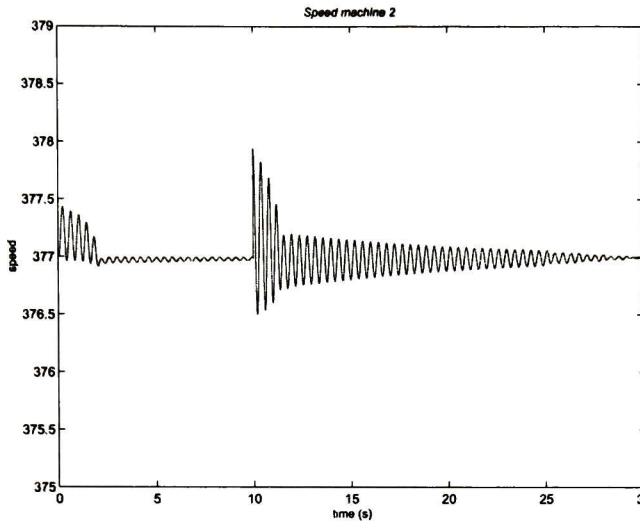

Figure 5.11: Rotor speed time evolution for machine 2

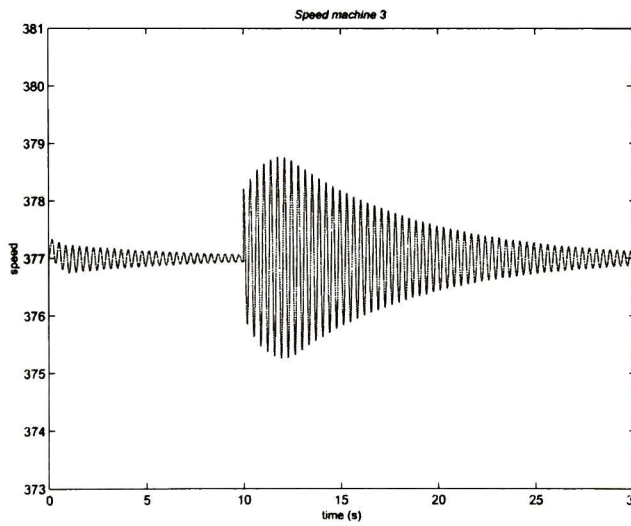

Figure 5.12: Rotor speed time evolution for machine 3

Chapter 6

Conclusions and Future Work

6.1 Conclusions

A decentralized neural identification and control scheme is proposed which is able to preserve stability for the whole system. The developed scheme is applied to different nonlinear electromechanical interconnected systems whose dynamical models includes bounded interconnection terms. Each subsystem is modeled according to the block control technique, which allows to develop a sliding mode control law. The control action forces the closed loop trajectory to converge and to stay in the sliding manifold, which guarantees that the tracking error is zero.

A neural identifier with the same block controllable properties than the *ith* subsystem is proposed to approximate the subsystem dynamical models. The neural identifier does not includes the interconnection terms and is trained with only local information via a decentralized robust learning law. Updating weight law avoids the drift parameter phenomenon using the well known σ-modification. This modification allows to update the sinaptic weights with no persistency of excitation condition required.

We tested out our decentralized scheme using the following interconnection plants:

a) *Interconnected double inverted pendulum*: The identification error converges to zero and the weights parameters tends to fixed values. The control action allows regulation and tracking. As far as we know, for this plant, the tracking problem

is for the first time presented in this dissertation. External disturbances are rejected. The capabilities of the tracking performance depends strongly of the interconnection terms as we tested via simulations.

b) *Single machine infinite bus system (SMIB)*: We used an $8th$ order model to represent the SMIB. A reduced neural identifier based on the $3rd$ order neural model of the power system is proposed. A sliding mode controller is developed based on the reduced neural identifier. Simulation results presented good performance even in presence of a short circuit fault. Neural weight remains bounded and the identification error converges to a value very close to zero.

c) *Two machines infinite bus power system*: The decentralized scheme is simulated using a $3rd$ order model to represent this power system. The identification errors and the weights parameters remains bounded for the ith subsystem. A short circuit fault is simulated and the control action is able to regulate the angle of the machine i as well as the neural parameters. In simulations results, we noticed that the damping of the ith angle depends on the chosen neural parameters and the respective learning law. The angle damping performance can be modified by selecting such parameters adequately.

d) *WSCC power system*: A $6th$ order model representation is used. A $3rd$ order reduced model is proposed to approximate the subsystem dynamics. Simulations shows that the identification error and the neural weights remains bounded during simulation tests even in presence of a short circuit fault. The transient response of the machines shows a damping response which remains bounded and converges to the stable operation condition after an external disturbance is applied. It is worth to point out that the damping oscillations of the systems are strongly dependent on the neural network identifier parameters as well as the respective learning law, i.e., oscillations are dependent on the adaptive structures of the developed scheme.

6.2 Future work

The research could be proceed as:

- Due the fact that the interconnection terms are related with the way subsystems are obtained, then research is required to analyze the relationship between subsystems stability and the performance of the whole system when adaptive schemes are used.

- To analyze the stability of reduced neural identifiers as applied to large scale systems and the relation between the size of the systems and the number of states to be identified.

- To analyze the controllability of the neural identifier on the open loop stage in order to avoid the use of fixed parameter on the neural identifier.

- To develop an interconnected double inverted pendulum real-time application in order to test the decentralized proposed scheme.

- More research is required to verify the applicability of reduced adaptive identifiers to electric power systems under different disturbance conditions such as load chances and mechanical disturbances.

Appendix A

Synchronous Machine Modeling

This appendix introduces the synchronous machine model, and its physical characteristics. The main purpose on this appendix is to present the fundamentals of the synchronous generator in order to obtain the large-scale power system, named multi-machine model. This appendix is based on [2] and [24]

A.1 Construction and Principle of Operation

The three phase synchronous machine considered is shown in Fig.A.1. It consists of two parts: stator and rotor. Both, stator and rotor have windings; the stator winding is a three phase winding and is sometimes called the armature winding. The rotor winding is called the field winding, which is connected to supply through the slip rings and brushes. There are two types of rotors:

- Salient-pole rotor (Fig. A.1) for low-speed machines (e.g. hydro-generators)
- Cylindrical rotor (Fig. A.2) for hight-speed machines (e.g. turbo-generators)

The two basic structures mentioned depends on their respective usage. Hydraulic turbines operate at low speeds and hence a relative large number of poles are required to produce the required rated frequency. A rotor with salient or projecting poles and concentrated windings is better suited mechanically to this situation. Such rotors often have damper windings or amortisseurs in the form of copper or brass rods

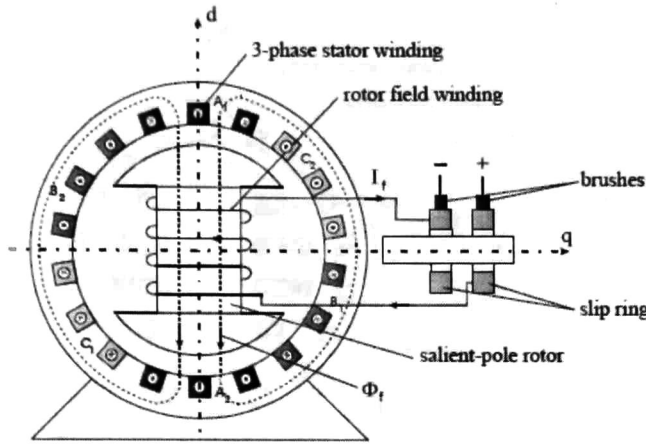

Figure A.1: Synchronous machine with salient-pole rotor

embedded in the pole face. These bars are connected to end ring to form short-circuited windings similar to those of squirrel cage induction motors, as shown in Fig. A.3. They are intended to dump out speed oscillations. Steam and gas turbines, on the other hand, operate at high speeds. Their generators have round (or cylindrical) rotors made up of solid steel forgings. They do not have special damper windings, but the solid steel rotor offers paths to eddy currents, which have effects equivalent to amortisseur currents.

A.1.1 Machines with multiple pole pairs

Machines with more than one pair of field poles have stator windings made up of a corresponding set of coils. For purposes of analysis, it is convenient to consider only a single pair of poles and consider that conditions associated with other pole pairs are identical to those for the pair under consideration. Therefore, angles are normally measured in electrical radians or degrees. The angle covered by one pole pair p_f is 2π radians or 360 electrical degrees. The relationship between the electrical angle θ and the corresponding mechanical angle θ_m is

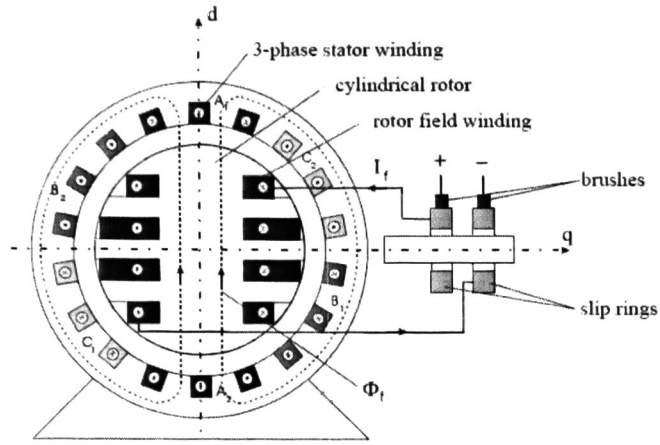

Figure A.2: Synchronous machine with cylindrical rotor

$$\theta = \frac{p_f}{2}\theta_m \tag{A.1}$$

MMF Waveforms

The armature windings and round rotor machine field windings are distributed in many slots so that the resulting mmf and flux waveforms have nearly sinusoidal space distribution. Let us consider, the mmf waveform due to armature windings only. The mmf produced by current flowing in only one coil in phase a is illustrated in Fig. A.4 in which the cross section of the stator has been cut open and rolled out in order to view of the mmf wave. By adding more coils, a sinusoidal mmf wave distribution is obtained. Machine design [10] aims at minimizing harmonics and, for most analysis of machine performance, it is reasonable to assume that each phase winding produce a sinusoidally distributed mmf wave.

Rotating magnetic field

The net mmf wave due to the three phase windings in the stator of phase a may be described as follows

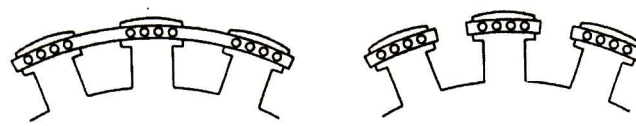

Figure A.3: Salient pole rotor construction

$$\begin{aligned} MMF_a &= Ki_a \cos(\gamma) \\ MMF_b &= Ki_b \cos\left(\gamma - \frac{2\pi}{3}\right) \\ MMF_c &= Ki_c \cos\left(\gamma + \frac{2\pi}{3}\right) \end{aligned} \tag{A.2}$$

where γ representing the angle along the periphery of the stator with respect to the center of phase a;

i_a, i_b and i_c are the instantaneous values of the phase currents and K is a constant. The three mmf waves due to the three phases are displaced 120 electrical degrees apart in space.

With balanced phase currents, and time origin arbitrary chosen as the instant when i_a is maximum, we have

$$\begin{aligned} i_a &= I_m \cos(\omega_s t) \\ i_b &= I_m \cos\left(\omega_s t - \frac{2\pi}{3}\right) \\ i_c &= I_m \cos\left(\omega_s t + \frac{2\pi}{3}\right) \end{aligned} \tag{A.3}$$

where $\omega_s = 2\pi f$ = angular frequency of stator currents in electrical degrees rad/s. The total mmf due to the three phases is given by

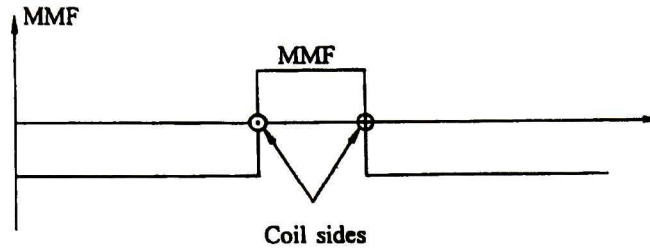

Figure A.4: MMF due to a single coil

$$
\begin{aligned}
MMF_{total} &= MMF_a + MMF_b + MMF_c \\
&= KI_m \left[\cos(\omega_s t)\cos\gamma + \cos\left(\omega_s t - \frac{2\pi}{3}\right)\cos\left(\gamma - \frac{2\pi}{3}\right)\right] + \\
&\quad \cos\left(\omega_s t + \frac{2\pi}{3}\right)\cos\left(\gamma + \frac{2\pi}{3}\right) \qquad \text{(A.4)} \\
&= \frac{3}{2} KI_m \cos(\gamma - \omega_s t)
\end{aligned}
$$

This is the equation of a traveling wave. At any instant in time, the total mmf has a sinusoidal spatial distribution; it has a constant amplitude and space–phase angle ωst_s which is function of time. Thus, the entire mmf wave moves at the constant angular velocity of ω_s electrical rad/s.

The magnitude of the stator mmf wave and its relative angular position with respect to the rotor mmf wave depend on the synchronous machine load (output). The electromagnetic torque on the rotor acts in a direction so as to bring the magnetic field into alignment. If the rotor field leads the armature field, the torque acts in opposition to the rotation with the machine acting as a generator. On the other hand, if the rotor field lags the armature field, the torque acts in the direction of rotation with the machine acting as a motor.

Direct and quadrature axis

The magnetic circuits and all rotor windings are symmetrical with respect to both polar axis. For the purpose of finding out synchronous machine characteristics, two

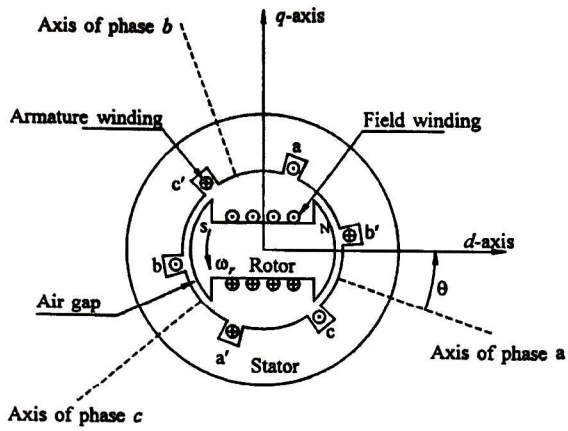

Figure A.5: MMF due to a single coil

axes are defined as shown in Fig. A.5.

- The direct (d) axis, centered magnetically in the center of north pole;
- The quadrature (q) axis, 90 electrical degrees ahead of the d-axis.

The position of the rotor relative to the stator is measured by the angle θ between the d-axis and the magnetic axis of phase a winding [20].

A.2 Synchronous Machine Model

The basic dynamic equations for a balanced, symmetrical, three-phase synchronous machine with a field winding and three damper windings on the rotor is presented.

The stator circuits consist of three-phase armature windings carrying alternating currents. The rotor circuits comprise field and amortisseur windings. The field win-

ding is connected to a source of direct current. In machine design analysis, a large number of circuits are used to represent amortisseur effects. For system analysis, where the characteristics of the machines as seen from its stator and rotor terminals are of interest, a limited number of circuits may be used.

The fundamental Kirchhoff's, Faraday's and Newton's laws give

$$\begin{aligned}
v_a &= i_a r_s + \frac{d\lambda_a}{dt} \\
v_b &= i_b r_s + \frac{d\lambda_b}{dt} \\
v_c &= i_c r_s + \frac{d\lambda_c}{dt} \\
v_{fd} &= i_{fd} r_{fd} + \frac{d\lambda_{fd}}{dt} \\
v_{1d} &= i_{1d} r_{1d} + \frac{d\lambda_{1d}}{dt} \\
v_{1q} &= i_{1q} r_{1q} + \frac{d\lambda_{1q}}{dt} \\
v_{2q} &= i_{2q} r_{2q} + \frac{d\lambda_{2q}}{dt} \\
\frac{d\theta}{dt} &= \omega \\
J\frac{d\omega}{dt} &= T_m - T_e - T_{fw}
\end{aligned} \tag{A.5}$$

where λ is flux linkage, r is winding resistance, J is the inertia constant, T_m is the mechanical torque applied to the shaft, T_e is the electrical torque, and T_{fw} is a friction windage torque.

A.3 Transformations and Scaling

Equations (A.5), completely describe the electrical performance of a synchronous machine. However, these equations contain inductance terms which vary with angle θ, which in turn varies with time. This introduces considerable complexity in solving machine and power system problems. A much simpler model is obtained by appropriated transformation of stator variables. [23]:

$$v_{dq0} \triangleq T_{dq0} v_{abc}, \quad i_{dq0} \triangleq T_{dq0} i_{abc}, \quad \lambda_{dq0} \triangleq T_{dq0} \lambda_{abc} \tag{A.6}$$

where

$$v_{abc} \triangleq \begin{bmatrix} v_a & v_b & v_c \end{bmatrix}^T, \quad i_{abc} = \begin{bmatrix} i_a & i_b & i_c \end{bmatrix}^T \quad \lambda_{abc} = \begin{bmatrix} \lambda_a & \lambda_b & \lambda_c \end{bmatrix}^T \tag{A.7}$$

$$v_{dq0} \triangleq \begin{bmatrix} v_d & v_q & v_0 \end{bmatrix}^T, \quad i_{dq0} = \begin{bmatrix} i_d & i_q & i_0 \end{bmatrix}^T \quad \lambda_{dq0} = \begin{bmatrix} \lambda_d & \lambda_q & \lambda_0 \end{bmatrix}^T \tag{A.8}$$

and

$$T_{dq0} \triangleq \frac{2}{3} \begin{bmatrix} \sin\theta & \sin\left(\theta - \frac{2\pi}{3}\right) & \cos\left(\theta + \frac{2\pi}{3}\right) \\ \cos\theta & \cos\left(\theta - \frac{2\pi}{3}\right) & \cos\left(\theta + \frac{2\pi}{3}\right) \\ \frac{1}{2} & \frac{1}{2} & \frac{1}{2} \end{bmatrix} \tag{A.9}$$

with the inverse

$$T_{dq0}^{-1} \triangleq \begin{bmatrix} \sin\theta & \cos\theta & 1 \\ \sin\left(\theta - \frac{2\pi}{3}\right) & \cos\left(\theta - \frac{2\pi}{3}\right) & 1 \\ \sin\left(\theta + \frac{2\pi}{3}\right) & \cos\left(\theta + \frac{2\pi}{3}\right) & 1 \end{bmatrix} \tag{A.10}$$

From (A.5), Kirchhoff's and Faraday's laws are

$$v_{abc} = r_s i_{abc} + \frac{d}{dt}\left(\lambda_{abc}\right) \tag{A.11}$$

which, when transformed using (A.9) and (A.10), are

$$v_{dq0} = r_s i_{dq0} + T_{dq0} \frac{d}{dt}\left(T_{dq0}^{-1} \lambda_{dq0}\right) \tag{A.12}$$

The system in $dq0$ coordinates has the forms

$$\begin{aligned}
v_d &= r_s i_d - \omega\lambda_q + \frac{d\lambda_d}{dt} \\
v_q &= r_s i_q + \omega\lambda_d + \frac{d\lambda_q}{dt} \\
v_0 &= r_s i_0 + \frac{d\lambda_0}{dt} \\
v_{fd} &= r_{fd} i_{fd} + \frac{d\lambda_{fd}}{dt} \\
v_{1d} &= r_{1d} i_{1d} + \frac{d\lambda_{1d}}{dt} \\
v_{1q} &= r_{1q} i_{1q} + \frac{d\lambda_{1q}}{dt} \\
v_{2q} &= r_{2q} i_{2q} + \frac{d\lambda_{2q}}{dt} \\
\frac{d\theta}{dt} &= \omega \\
J\frac{d\omega}{dt} &= T_m - T_e - T_{fw}
\end{aligned} \tag{A.13}$$

To derive an expression for T_e, it is necessary to look at the overall energy for the machine. After analyzing the power balance energy [33], T_e is obtained as

$$T_e = -(\lambda_d i_q - \lambda_q i_d) \tag{A.14}$$

To complete the dynamical model in the transformed variables, the angle is defined as

$$\delta \triangleq \theta - \omega_s t \tag{A.15}$$

where ω_s is a constant normally called rated synchronous speed in electrical radians per second, giving

$$\frac{d\delta}{dt} = \omega - \omega_s \tag{A.16}$$

A.3.1 Per-unit system

It is usual to scale the synchronous machine model using the traditional concept of per-unit [31], [16]. The new $dq0$ variables are defined as

$$\begin{aligned} V_d &\triangleq \tfrac{v_d}{V_{BDQ}}, \quad V_q \triangleq \tfrac{v_q}{V_{BDQ}}, \quad V_0 \triangleq \tfrac{v_0}{V_{BDQ}}, \\ I_d &\triangleq \tfrac{-i_d}{I_{BDQ}}, \quad I_q \triangleq \tfrac{-i_q}{I_{BDQ}}, \quad I_0 \triangleq \tfrac{-i_0}{I_{BDQ}}, \\ \psi_d &\triangleq \tfrac{\lambda_d}{\Lambda_{BDQ}}, \quad \psi_q \triangleq \tfrac{\lambda_q}{\Lambda_{BDQ}}, \quad \psi_0 \triangleq \tfrac{\lambda_0}{\Lambda_{BDQ}} \end{aligned} \tag{A.17}$$

where V_{BDQ} is the rated peak line to neutral voltage, and

$$I_{BDQ} \triangleq \tfrac{2S_B}{3V_{BDQ}}, \quad \Lambda_{BDQ} \triangleq \tfrac{V_{BDQ}}{\omega_B} \tag{A.18}$$

with S_B and ω_B equal to the rated speed in electrical radians per second (ω_s). The new rotor variables are defined as

$$\begin{aligned} V_{fd} &\triangleq \tfrac{v_{fd}}{V_{BFD}}, \quad V_{1d} \triangleq \tfrac{v_{1d}}{V_{B1D}}, \quad V_{1q} \triangleq \tfrac{v_{1q}}{V_{B1Q}} \quad V_{2q} \triangleq \tfrac{v_{2q}}{V_{B2Q}}, \\ I_{fd} &\triangleq \tfrac{i_{fd}}{I_{BFD}}, \quad I_{1d} \triangleq \tfrac{i_{1d}}{I_{B1D}}, \quad I_{1q} \triangleq \tfrac{i_{1q}}{I_{B1Q}}, \quad I_{2q} \triangleq \tfrac{i_{2q}}{I_{B2Q}}, \\ \psi_{fd} &\triangleq \tfrac{\lambda_{fd}}{\Lambda_{BFD}}, \quad \psi_{1d} \triangleq \tfrac{\lambda_{1d}}{\Lambda_{B1D}}, \quad \psi_{1q} \triangleq \tfrac{\lambda_{1q}}{\Lambda_{B1Q}}, \quad \psi_{2q} \triangleq \tfrac{\lambda_{2q}}{\Lambda_{B2Q}} \end{aligned} \tag{A.19}$$

where the rotor circuit base voltage and base flux linkages are respectively

$$\begin{aligned} V_{BFD} &\triangleq \tfrac{S_B}{I_{BFD}}, \quad V_{B1D} \triangleq \tfrac{S_B}{I_{B1D}}, \quad V_{B1Q} \triangleq \tfrac{S_B}{I_{B1Q}}, \quad V_{B2Q} \triangleq \tfrac{S_B}{I_{B1Q}}, \\ \Lambda_{BFD} &\triangleq \tfrac{V_{BFD}}{\omega_B}, \quad \Lambda_{B1D} \triangleq \tfrac{V_{B1D}}{\omega_B}, \quad \Lambda_{B1Q} \triangleq \tfrac{V_{B1Q}}{\omega_B}, \quad \Lambda_{B2Q} \triangleq \tfrac{V_{B2Q}}{\omega_B} \end{aligned} \tag{A.20}$$

The model parameters are scaled as follows

$$R_s \triangleq \tfrac{r_s}{Z_{BDQ}}, \quad R_{fd} \triangleq \tfrac{r_{fd}}{Z_{BFD}}, \quad R_{1d} \triangleq \tfrac{r_{1d}}{Z_{B1D}}, \quad R_{1q} \triangleq \tfrac{r_{1q}}{Z_{B1Q}}, \quad R_{2q} \triangleq \tfrac{r_{2q}}{Z_{B2Q}} \tag{A.21}$$

with

$$\begin{aligned} Z_{BDQ} &\triangleq \tfrac{V_{BDQ}}{I_{BDQ}}, \quad Z_{BFD} \triangleq \tfrac{V_{BFD}}{I_{BFD}}, \quad Z_{B1D} \triangleq \tfrac{V_{B1D}}{I_{B1D}}, \\ Z_{B1Q} &\triangleq \tfrac{V_{B1Q}}{I_{B1Q}}, \quad Z_{B2Q} \triangleq \tfrac{V_{B2Q}}{I_{B2Q}} \end{aligned} \tag{A.22}$$

The shaft inertia constant and shaft torque are scaled by defining

$$H \triangleq \frac{\frac{1}{2}J\left(\omega_B\right)^2}{S_B} \tag{A.23}$$

$$T_M \triangleq \frac{T_m}{T_B}, \quad T_{FW} \triangleq \frac{T_{fw}}{T_B}, \quad T_B \triangleq \frac{S_B}{\omega_B} \tag{A.24}$$

The synchronous machine equations, using the scaled variables with $\omega_B = \omega_s$ are

$$\begin{aligned}
\frac{1}{\omega_s}\frac{d\psi_d}{dt} &= R_s I_d + \frac{\omega}{\omega_s}\psi_q + V_d \\
\frac{1}{\omega_s}\frac{d\psi_q}{dt} &= R_s I_q - \frac{\omega}{\omega_s}\psi_d + V_q \\
\frac{1}{\omega_s}\frac{d\psi_0}{dt} &= R_s I_0 + V_0 \\
\frac{1}{\omega_s}\frac{d\psi_{fd}}{dt} &= -R_{fd} I_{fd} + V_{fd} \\
\frac{1}{\omega_s}\frac{d\psi_{1d}}{dt} &= -R_{1d} I_{1d} + V_{1d} \\
\frac{1}{\omega_s}\frac{d\psi_{1q}}{dt} &= -R_{1q} I_{1q} + V_{1q} \\
\frac{1}{\omega_s}\frac{d\psi_{2q}}{dt} &= -R_{2q} I_{2q} + V_{2q} \\
\frac{d\delta}{dt} &= \omega - \omega_s \\
\frac{2H}{\omega_s} &= T_M - (\psi_d I_q - \psi_q I_d) - T_{FW}
\end{aligned} \tag{A.25}$$

In order to obtain (A.25), the following assumptions must be fulfilled

1. The stator has three coils in a balanced symmetrical configuration centered 120 electrical degrees apart.

2. The rotor has four coils in a balanced symmetrical configuration located in pairs 90 electrical degrees apart.

3. The relationship between the flux linkages and currents must reflect a conservative coupling field.

4. The relationship between the flux linkages and currents must be independent of θ when expressed in the $dq0$ coordinate system.

The following section give the flux linkage/current relationships, which satisfy these four assumptions and thus complete the dynamical model.

A.4 The Linear Magnetic Circuit

This section presents the treatment of the case in which the machine flux linkage are assumed to be linear functions of currents:

$$\lambda_{abc} = L_{ss}(\theta)\, i_{abc} + L_{sr}(\theta)\, i_R \tag{A.26}$$

$$\lambda_R = L_{rs}(\theta)\, i_{abc} + L_{rr}(\theta)\, i_R \tag{A.27}$$

where

$$i_R \triangleq \left[\begin{array}{cccc} i_{fd} & i_{1d} & i_{1q} & i_{2q} \end{array}\right]^T \quad \lambda_R \triangleq \left[\begin{array}{cccc} \lambda_{fd} & \lambda_{1d} & \lambda_{1q} & \lambda_{2q} \end{array}\right]^T \tag{A.28}$$

The inductance matrices which satisfy assumptions 3 and 4 are

$$L_{ss}(\theta) \triangleq \left[\begin{array}{ccc} L_{11} & L_{12} & L_{13} \\ L_{21} & L_{22} & L_{23} \\ L_{31} & L_{32} & L_{33} \end{array}\right] \tag{A.29}$$

with

$$\begin{aligned}
&L_{11} = L_{ls} + L_A - L_B\cos\theta, \quad L_{12} = -\tfrac{1}{2}L_A - L_B\cos\left(\theta - \tfrac{2\pi}{3}\right) \\
&L_{13} = -\tfrac{1}{2}L_A - L_B\cos\left(\theta + \tfrac{2\pi}{3}\right), \quad L_{21} = -\tfrac{1}{2}L_A - L_B\cos\left(\theta - \tfrac{2\pi}{3}\right), \\
&L_{22} = L_{ls} + L_A - L_B\cos\left(\theta + \tfrac{2\pi}{3}\right) \quad L_{23} = -\tfrac{1}{2}L_A - L_B\cos\theta, \\
&L_{31} = -\tfrac{1}{2}L_A - L_B\cos\left(\theta + \tfrac{2\pi}{3}\right), \quad L_{32} = -\tfrac{1}{2}L_A - L_B\cos\theta, \\
&L_{33} = L_{ls} + L_A - L_B\cos\left(\theta - \tfrac{2\pi}{3}\right)
\end{aligned}$$

$$L_{sr}(\theta) = L_{rs}^T \triangleq \left[\begin{array}{cccc} \hat{L}_{11} & \hat{L}_{12} & \hat{L}_{13} & \hat{L}_{14} \\ \hat{L}_{21} & \hat{L}_{22} & \hat{L}_{23} & \hat{L}_{24} \\ \hat{L}_{31} & \hat{L}_{32} & \hat{L}_{33} & \hat{L}_{34} \end{array}\right] \tag{A.30}$$

$$\begin{aligned}
&\hat{L}_{11} = L_{sfd}\sin\theta, \quad \hat{L}_{12} = L_{s1d}\sin\theta, \\
&\hat{L}_{13} = L_{s1q}\cos\theta, \quad \hat{L}_{14} = L_{s2q}\cos\theta, \\
&\hat{L}_{21} = L_{sfd}\sin\left(\theta - \tfrac{2\pi}{3}\right). \quad \hat{L}_{22} = L_{s1d}\sin\left(\theta - \tfrac{2\pi}{3}\right) \\
&\hat{L}_{23} = L_{s1q}\cos\left(\theta - \tfrac{2\pi}{3}\right), \quad \hat{L}_{24} = L_{s2q}\cos\left(\theta - \tfrac{2\pi}{3}\right), \\
&\hat{L}_{31} = L_{sfd}\sin\left(\theta + \tfrac{2\pi}{3}\right), \quad \hat{L}_{32} = L_{s1d}\sin\left(\theta + \tfrac{2\pi}{3}\right), \\
&\hat{L}_{33} = L_{s1q}\cos\left(\theta + \tfrac{2\pi}{3}\right), \quad \hat{L}_{34} = L_{s2q}\cos\left(\theta + \tfrac{2\pi}{3}\right)
\end{aligned}$$

$$L_{rr}(\theta) \triangleq \begin{bmatrix} L_{fdfd} & L_{fd1d} & 0 & 0 \\ L_{fd1d} & L_{1d1d} & 0 & 0 \\ 0 & 0 & L_{1q1q} & L_{1q2q} \\ 0 & 0 & L_{1q2q} & L_{2q2q} \end{bmatrix} \tag{A.31}$$

After using (A.7) the set of flux linkage/currents are obtained as

$$\begin{aligned} \lambda_d &= (L_{ls} + L_{md})\, i_d + L_{sfd} i_{fd} + L_{s1d} i_{1d} \\ \lambda_{fd} &= \frac{3}{2} L_{sfd} i_d + L_{fdfd} i_{fd} + L_{fd1d} i_{1d} \\ \lambda_{1d} &= \frac{3}{2} L_{s1d} i_d + L_{fd1d} i_{fd} + L_{1d1d} i_{1d} \\ \lambda_q &= (L_{ls} + L_{mq})\, i_q + L_{s1q} i_{1q} + L_{s2q} i_{2q} \\ \lambda_{1q} &= \frac{3}{2} L_{s1q} i_q + L_{1q1q} i_{1q} + L_{1q2q} i_{2q} \\ \lambda_{2q} &= \frac{3}{2} L_{s2q} i_q + L_{1q2q} i_{1q} + L_{2q2q} i_{2q} \\ \lambda_0 &= L_{ls} i_0 \end{aligned} \tag{A.32}$$

Using the scaled quantities the fluxes are

$$\begin{aligned} \psi_d &= \frac{\omega_s (L_{ls} + L_{md})(-I_d I_{BDQ})}{V_{BDQ}} + \frac{\omega_s L_{sfd} I_{fd} I_{BFD}}{V_{BDQ}} + \frac{\omega_s L_{s1d} I_{1d} I_{B1D}}{V_{BDQ}} \\ \psi_{fd} &= \frac{\omega_s \frac{3}{2} L_{sfd}(-I_d I_{BDQ})}{V_{BFD}} + \frac{\omega_s L_{fdfd} I_{fd} I_{BFD}}{V_{BFD}} + \frac{\omega_s L_{fd1d} I_{1d} I_{B1D}}{V_{BFD}} \\ \psi_{1d} &= \frac{\omega_s \frac{3}{2} L_{s1d}(-I_d I_{BDQ})}{V_{B1D}} + \frac{\omega_s L_{fd1d} I_{fd} I_{BFD}}{V_{B1D}} + \frac{\omega_s L_{1d1d} I_{1d} I_{B1D}}{V_{B1D}} \\ \psi_q &= \frac{\omega_s (L_{ls} + L_{mq})(-I_q I_{BDQ})}{V_{BDQ}} + \frac{\omega_s L_{s1q} I_{1q} I_{B1Q}}{V_{BDQ}} + \frac{\omega_s L_{s2q} I_{2q} I_{B2Q}}{V_{BDQ}} \\ \psi_{1q} &= \frac{\omega_s \frac{3}{2} L_{s1q}(-I_q I_{BDQ})}{V_{B1Q}} + \frac{\omega_s L_{1q1q} I_{1q} I_{B1Q}}{V_{B1Q}} + \frac{\omega_s L_{1q2q} I_{2q} I_{B2Q}}{V_{B1Q}} \\ \psi_{2q} &= \frac{\omega_s \frac{3}{2} L_{s2q}(-I_q I_{BDQ})}{V_{B2Q}} + \frac{\omega_s L_{1q2q} I_{1q} I_{B1Q}}{V_{B2Q}} + \frac{\omega_s L_{2q2q} I_{2q} I_{B2Q}}{V_{B2Q}} \\ \psi_0 &= \frac{\omega_s L_{ls}(-I_0 I_{BDQ})}{V_{BDQ}} \end{aligned} \tag{A.33}$$

with

$$\begin{aligned} I_{BFD} &\triangleq \tfrac{L_{md}}{L_{sfd}} I_{BDQ}, \quad I_{B1D} \triangleq \tfrac{L_{md}}{L_{s1d}} I_{BDQ} \\ I_{B1Q} &\triangleq \tfrac{L_{mq}}{L_{s1q}} I_{BDQ}, \quad I_{B2Q} \triangleq \tfrac{L_{mq}}{L_{s2q}} I_{BDQ} \end{aligned} \tag{A.34}$$

and the following scaled parameters

$$\begin{aligned}
&X_{ls} \triangleq \tfrac{\omega_s L_{ls}}{Z_{BDQ}}, \quad X_{md} \triangleq \tfrac{\omega_s L_{md}}{Z_{BDQ}}, \quad X_{mq} \triangleq \tfrac{\omega_s L_{mq}}{Z_{BDQ}}, \\
&X_{md} \triangleq \tfrac{\omega_s L_{fdfd}}{Z_{BFD}}, \quad X_{1d} \triangleq \tfrac{\omega_s L_{1d1d}}{Z_{B1D}}, \quad X_{fd1d} \triangleq \tfrac{\omega_s L_{fd1d}}{Z_{BFD} L_{s1d}}, \\
&X_{1q} \triangleq \tfrac{\omega_s L_{1q1q}}{Z_{B1Q}}, \quad X_{2q} \triangleq \tfrac{\omega_s L_{2q2q}}{Z_{B2Q}}, \quad X_{1q2q} \triangleq \tfrac{\omega_s L_{1q2q} L_{s1q}}{Z_{B1Q} L_{s2q}}
\end{aligned} \tag{A.35}$$

The scaled leakage reactances of the rotor winding are defined as

$$\begin{aligned}
&X_{lfd} \triangleq X_{fd} - X_{md}, \quad X_{l1d} \triangleq X_{1d} - X_{md}, \\
&X_{l1q} \triangleq X_{1q} - X_{mq}, \quad X_{2q} \triangleq X_{2q} - X_{mq}, \\
&X_d \triangleq X_{ls} + X_{md}, \quad X_q \triangleq X_{ls} + X_{mq}
\end{aligned} \tag{A.36}$$

The resulting scaled $\psi - I$ relationship is

$$\begin{aligned}
\psi_d &= X_d(-I_d) + X_{md} I_{fd} + X_{md} I_{1d} \\
\psi_{fd} &= X_{md}(-I_d) + X_{fd} I_{fd} + X_{md} I_{1d} \\
\psi_{1d} &= X_{md}(-I_d) + X_{md} I_{fd} + X_{1d} I_{1d} \\
\psi_q &= X_q(-I_q) + X_{mq} I_{1q} + X_{mq} I_{2q} \\
\psi_{1q} &= X_{mq}(-I_q) + X_{1q} I_{1q} + X_{mq} I_{2q} \\
\psi_{2q} &= X_{mq}(-I_q) + X_{mq} I_{1q} + X_{2q} I_{2q} \\
\psi_0 &= X_{ls}(-I_0)
\end{aligned} \tag{A.37}$$

It is common to define the following parameters

$$\begin{aligned}
&X''_d \triangleq X_{ls} + \tfrac{1}{\frac{1}{X_{md}} + \frac{1}{X_{lfd}} + \frac{1}{X_{l1d}}}, \quad X''_q \triangleq X_{ls} + \tfrac{1}{\frac{1}{X_{mq}} + \frac{1}{X_{l1q}} + \frac{1}{X_{l2q}}}, \\
&X'_d \triangleq X_d - \tfrac{X_{md}^2}{X_{fd}}, \quad X'_q \triangleq X_q - \tfrac{X_{mq}^2}{X_{1q}}, \\
&T'_{d0} \triangleq \tfrac{X_{fd}}{\omega_s R_{fd}}, \quad T'_{q0} \triangleq \tfrac{X_{1q}}{\omega_s R_{1q}}, \\
&T''_{d0} \triangleq \tfrac{1}{\omega_s R_{1d}} \left(X_{l1d} + \tfrac{1}{\frac{1}{X_{md}} + \frac{1}{X_{lfd}}} \right) \quad T''_{q0} \triangleq \tfrac{1}{\omega_s R_{2q}} \left(X_{l2q} + \tfrac{1}{\frac{1}{X_{mq}} + \frac{1}{X_{l1q}}} \right)
\end{aligned} \tag{A.38}$$

and the following variables

$$\begin{aligned} E'_q &\triangleq \frac{X_{md}}{X_{fd}}\psi_{fd} \\ E_{fd} &\triangleq \frac{X_{md}}{R_{fd}}V_{fd} \\ E'_d &\triangleq -\frac{X_{mq}}{X_{1q}}\psi_{1q} \end{aligned} \tag{A.39}$$

Using (A.38) and (A.39), equations (A.37) can be expressed as

$$\begin{aligned} \psi_d &= -X''_d I_d + \frac{(X''_d - X_{ls})}{(X'_d - X_{ls})}E'_q + \frac{(X'_d - X''_d)}{(X'_d - X_{ls})}\psi_{1d} \\ I_{fd} &= \frac{1}{X_{md}}\left[E'_q + (X_d - X'_d)(I_d - I_{1d})\right] \\ I_{1d} &= \frac{X'_d - X''_d}{(X'_d - X_{ls})^2}\left[\psi_{1d} + (X'_d - X_{ls})I_d - E'_q\right] \\ \psi_q &= -X''_q I_q - \frac{(X''_d - X_{ls})}{(X'_q - X_{ls})}E'_d + \frac{(X'_q - X''_q)}{(X'_q - X_{ls})}\psi_{2q} \\ I_{1q} &= \frac{1}{X_{mq}}\left[-E'_d + (X_q - X'_q)(I_q - I_{2q})\right] \\ I_{2q} &= \frac{X'_q - X''_q}{(X'_q - X_{ls})^2}\left[\psi_{2q} + (X'_q - X_{ls})I_q + E'_d\right] \\ \psi_0 &= -X_{ls}I_0 \end{aligned} \tag{A.40}$$

Substituting (A.40) into (A.25) gives the synchronous machine dynamical model

as

$$
\begin{aligned}
\frac{d\delta}{dt} &= \omega - \omega_s \\
\frac{2H}{\omega_s}\frac{d\omega}{dt} &= T_M - (\psi_d I_q - \psi_q I_d) \\
T'_{d0}\frac{dE'_q}{dt} &= -E'_q - (X_d - X'_d)\left[I_d - \frac{X'_d - X''_d}{(X'_d - X_{ls})^2}\left(\psi_{1d} + (X'_d - X_{ls})\, I_d - E'_q\right)\right] + E_{fd} \\
T'_{q0}\frac{dE'_d}{dt} &= -E'_d + (X_q - X'_q)\left[I_q - \frac{X'_q - X''_q}{(X'_q - X_{ls})^2}\left(\psi_{2q} + (X'_q - X_{ls})\, I_q + E'_d\right)\right] \\
T''_{d0}\frac{d\psi_{1d}}{dt} &= -\psi_{1d} + E'_q - (X'_d - X_{ls})\, I_d \qquad \text{(A.41)} \\
T''_{q0}\frac{d\psi_{2q}}{dt} &= -\psi_{2q} - E'_d - (X'_q - X_{ls})\, I_q \\
\psi_d &= -X''_d I_d + \frac{(X''_d - X_{ls})}{(X'_d - X_{ls})}E'_q + \frac{(X'_d - X''_d)}{(X'_d - X_{ls})}\psi_{1d} \\
\psi_q &= -X''_q I_q - \frac{(X''_d - X_{ls})}{(X'_q - X_{ls})}E'_d + \frac{(X'_q - X''_q)}{(X'_q - X_{ls})}\psi_{2q}
\end{aligned}
$$

Appendix B

Publications

B.1 Journal papers

- V.H. Benitez, E.N. Sanchez and A.G. Loukianov, Reduced order neural block control for synchronous electric generator. *Dynamics of Continuous, Discrete and Impulsive Systems. Series B: Applications and Algorithms,* vol. 15, no. 1, pp. 43-56, 2008.

- V H. Benitez, E. N. Sanchez and A. G. Loukianov, Decentralized Adaptive Recurrent Neural Control Structure. *Engineering Applications of Artificial Intelligence,* vol. 20, no. 8, pp. 1125-1132, 2007.

B.2 Conference papers

- V. H. Benitez, E. N. Sanchez and A. G. Loukianov, Decentralized neural control structure applied to large scale power systems, *Workshop on Modelling and Control of Complex Systems 2005,* Ayia Napa, Cyprus, June, 2005.

- V. H. Benitez, E. N. Sanchez and A. G. Loukianov, Decentralized neural control structure, *16th IFAC World Congress 2005,* Prague, Czech Republic, July, 2005.

- V. H. Benitez, E. N. Sanchez and A. G. Loukianov, Neural block control for a synchronous electric generator *International Joint Conference on Neural Networks 2004,* Budapest, Hungary, July, 2004.

Bibliography

[1] A. Y. Alanis, *Discrete-time Neural Control: Application to Induction Motors*, Ph. D. Dissertation, Cinvestav, Unidad Guadalajara, Guadalajara, Jalisco, Mexico, 2007.

[2] P. M. Anderson and A.A. Fouad, *Power System Control and Stability*, IEEE Press., New York, USA, 1994.

[3] V. H. Benitez, E.N. Sanchez and A.G. Loukianov, "Decentralized Adaptive Recurrent Neural Control Structure" *Engineering Applications of Artificial Intelligence,* vol. 20, no. 8, pp. 1125-1132, 2007.

[4] V. H. Benitez, A. G. Loukianov and E. N. Sanchez, "Neural identification and control of a linear induction motor using an $\alpha - \beta$ model", in *Proceedings of the American Control Conference*, Denver, Colorado, USA, pp. 4041-4046, 2003.

[5] E. H. Bristol "On a new measure of interactions for multivariable process control" *IEEE Trans. Autom. Control,* vol. 11, pp. 133-134, 1966.

[6] X. B. Chen, D.D. Siljak and S.S. Stankovic, "Decentralized control of multi-area multi-machine overlapping interconnected power systems", in *Proc. of International Conference on Control Theory and Applications 2001*, pp. 420-424, Pretoria, South Africa, 2001.

[7] X. B. Chen and S.S. Stankovic, "Overlapping decomposition and decentralized LQG control for interconnected power systems" in *Proceedings of IEEE SMC'96*, vol. 3, pp. 1904-1909, Beijing, China, 1996.

[8] N. E. Cotter, "The Stone-Weiertrass theorem and its application to neural networks" *IEEE Transactions on Neural Networks*, vol. 1, no. 4, pp. 290-295, 1990.

[9] T. W. Chow and Y. Fang, "A recurrent neural network based real-time learning control strategy applying to nonlinear systems with unknown dynamics," *IEEE Transactions on Industrial Electronics*, vol. 45, no. 1, pp. 151-161, 1998.

[10] R. D. Dunlop, R.M. Maliszewski and B.M. Pasternack, "Application of single phase switching on the AEP 765-kV system", in *Proceedings of the American Power Conference*, vol. 47, pp. 461-462, 1980.

[11] R. A. Felix, *Variable Structure Neural Control*, Ph. D. Dissertation, Cinvestav, Unidad Guadalajara, Guadalajara, Jalisco, Mexico, 2004.

[12] M. Galaz, R. Ortega, A Bazanella and A. Stankovic, "Excitation control of synchronous generators via total energy-shaping approach" in *Proceedings of American Control Conference*, pp. 817-821, Arlington, USA, 2001.

[13] D. T. Gavel and D. D. Siljak, "Decentralized adaptive control: structural conditions for stability." *IEEE Transactions on Automatic Control*, vol. 34, no. 4, 413-426. 1989.

[14] Y. Guo, D. J. Hill and Y. Wang, "Nonlinear decentralized control of large-scale power systems." *Automatica*, vol. 36, no. 9 pp. 1275-1289, 2000.

[15] K. E. Haggblom, "Control structure analysis by partial relative gains" in *Proceedings of the 36th IEEE Conference on Decision and Control*, vol. 3, pp. 2623-2624, San Diego, California, USA, 1997.

[16] M. R. Harris, P. J. Lawrenson and J. M. Stephenson, *Per-unit Systems with Special Reference to Electrical Machines*, Cambridge University Press, Cambridge, England, 1970.

[17] S. N. Huang, K. K. Tan and T. H. Lee, "Decentralized control design for large scale systems with strong interconnections using neural networks" *IEEE Transactions on Automatic Control*, vol. 48, no. 5, pp. 805-810, May 2003.

[18] S. Jain and F. Khorrami, "Decentralized control of large-scale power systems with unknown interconnections." in *Proceedings of the 4th IEEE Conference on Control Applications*, pp. 618-623, Brooklyn, Nueva York, USA, 1995.

[19] Z. P. Jiang, "New results in decentralized adaptive nonlinear control with output feedback." in *Proceedings of the 38th Conference on Decision and Control*, vol. 5, pp. 4772-4777, Phoenix, Arizona, USA, 1999.

[20] E. W. Kimbark, "Suppression of ground-fault arcs on single-pole switched EHV lines by shunt reactors" *IEEE Transactions on Power Apparatus and Systems* , vol. 83, no. 3 pp. 285-290, March 1964.

[21] E. B. Kosmatopoulus, M. A. Christodoulou and P. A. Ioannou, "Dynamical neural network that ensure exponential identification error convergence" *Neural Networks*, vol. 10, no. 2, pp. 299-314, 1997.

[22] E. B. Kosmatopoulus, M.M. Polycarpou, and P.A. Ioannou, "Higher order neural network structures for identification of dynamical systems" *IEEE Transactions on Neural Networks*, vol. 6, no. 2, pp. 422-431, 1995.

[23] P. C. Krause, *Analysis of Electric Machinery*, McGraw-Hill, New York, USA, 1986.

[24] P. Kundur, *Power System Stability and Control*, McGraw Hill, New York, USA, 1994.

[25] A. G. Loukianov, J.M. Canedo, V.I. Utkin and J. Cabrera-Vazquez, "Discontinuous controller for power systems: sliding-mode block control approach" *IEEE Transactions on Industrial Electronics*, vol. 51, no. 2, pp. 340-353, April 2004.

[26] A. G. Loukianov, "Robust block decomposition sliding mode control", *Mathematical Problems in Engineering*, vol. 8, no. 4-5, pp. 349-365, January 2003.

[27] A. G. Loukianov, "Nonlinear block control with sliding mode" *Automation and Remote Control*, vol. 57, no. 7, 916-933, 1998.

[28] F. Nardi, N. Hovakimyan and A.J. Calise, "Decentralized control of large-scale systems using single hidden layer neural networks." in *Proceedings of the American Control Conference*, vol. 4, pp. 3122-3127, Arlington, Virginia, USA, 2001.

[29] Y. M. Park, M. S. Choi and K. Y. Lee, "An Optimal tracking neuro-controller for nonlinear dynamic systems." *IEEE Transactions on Neural Networks*, vol. 7, no. 5, pp. 1099-1110, 1996.

[30] "Power System Dynamic Analysis-Phase I," *EPRI Report EL-484,* Electric Power Research Institute, July 1977.

[31] A. W. Rankin, "Per-unit impedance of synchronous machines," *AIEE Trans.,* vol. 64, pp. 569-573, 1945.

[32] G. A. Rovithakis and M.A Christodoulou, *Adaptive Control with Recurrent High-Order Neural Networks.* Springer-Verlag, London, England, 2000.

[33] P. W. Sauer and M. A. Pai, *Powers Systems Dynamics and Stability*, Prentice-Hall, New Jersey, USA, 1998.

[34] D. D. Siljak, *Decentralized Control of Complex Systems.* Academic Press, New York, USA, 1991.

[35] J. T. Spooner and K. M. Passino, "Decentralized adaptive control of nonlinear systems using radial basis neural networks" *IEEE Transactions on Automatic Control*, vol. 44, pp. 2050-2057, Nov. 1999.

[36] V. I. Utkin, *Sliding Modes in Control and Optimization*, Spriger Verlag, N.Y., USA, 1992.

CENTRO DE INVESTIGACIÓN Y DE ESTUDIOS AVANZADOS DEL I.P.N.
UNIDAD GUADALAJARA

El Jurado designado por la Unidad Guadalajara del Centro de Investigación y de Estudios Avanzados del Instituto Politécnico Nacional aprobó la tesis

Control Neuronal Descentralizado en Tiempo Continuo

del (la) C.

Victor Hugo BENITEZ BALTAZAR

el día 04 de Febrero de 2010.

Dr. Edgar Nelson Sánchez Camperos
Investigador CINVESTAV 3D
CINVESTAV Unidad Guadalajara

Dr. Juan Manuel Ramírez Arredondo
Investigador CINVESTAV 3C
CINVESTAV Unidad Guadalajara

Dr. Alexander Georgievich Loukianov
Investigador CINVESTAV 3C
CINVESTAV Unidad Guadalajara

Dr. Arturo Román Messina
Investigador CINVESTAV 3C
CINVESTAV Unidad Guadalajara

Dr. Antonio Ramírez Treviño
Investigador CINVESTAV 3A
CINVESTAV Unidad Guadalajara

Dra. Alma Yolanda Alanis García
Profesor
CUCEI UDG